Optimization of an All Normal Dispersion Fiber Laser and a Gain Managed Nonlinear Amplifier

by

Dean Eaton

A thesis

presented to the University Of Waterloo

in fulfillment of the

thesis requirement for the degree of

Master of Science

in

Physics

Waterloo, Ontario, Canada, 2023

Author's Declaration

I hereby declare that I am the sole author of this thesis. This is a true copy of the thesis, including any required final revisions, as accepted by my examiners.

I understand that my thesis may be made electronically available to the public.

Abstract

Ultrafast laser systems are used in a wide variety of modern laser research. The combination of an all-normal dispersion fiber laser and a gain-managed nonlinear fiber amplifier makes for inexpensive and easy to build system that can generate ultrashort pulses with high average power. In this thesis I explore the improvements and optimizations made to such a system for use in making a two-color laser amplifier system, to be used for projects such as multi-frequency Raman generation. An all-normal dispersion fiber mode-locked laser was developed for our group, but modifications were necessary to improve both the ease of mode-locking and extend the duration of self-sustaining. Spectral filtering is the key aspect of the mode-locking operations of an all-normal dispersion fiber laser and it is the mode-locking that generates the ultrashort pulses. This spectral filtering was optimized to improve the ease of mode-locking. The pulses at the output of the mode-locked laser were found to be too long to allow the maximum spectral broadening in the gain-managed nonlinear amplifier. Compression of these pulses with a grating compressor caused the amplified spectrum to be significantly broadened by the nonlinear optical interaction in the fiber. The resulting spectra of the nonlinear amplifier were analyzed as a function of seed power and pump power (up to an upper limit before the introduction of incoherent noise that seeds Raman scattering creating a red shoulder on the spectrum). The result of these investigations is an optimized laser system that produces a train of pulses with energy of 176nJ, a bandwidth exceeding 100nm, and an uncompressed pulse duration of approximately 6ps. The system can now deliver the needed energy and bandwidth for the two-color amplification experiments that will be conducted in the future with this laser system.

Acknowledgments

Acknowledgments are always difficult because it is impossible to express the full depth of gratitude I feel towards those who have supported me along the way. With that said, I would like to express my deepest gratitude to Dr. Donna Strickland for being an exceptional mentor and for providing me with the opportunity to work with her. Her guidance, encouragement, and patience have been invaluable throughout my master's degree journey, especially during the Covid-19 pandemic and the extra time it has taken me to complete this thesis and my degree.

I would also like to extend my appreciation to the other members of the research group, starting with Mingjian (Peter) Lyu, who has been an extraordinary source of knowledge, I have learned a great deal from him in terms of labs skills and critical thinking. I am also grateful to Samuel Laketa for his technical assistance and insightful discussions. Likewise, I am grateful to Reza Karimi for his assistance in coordinating various lab-related matters and assisting in helping me get oriented when I first started. I would like to thank my committee members, Dr. Joe Sanderson and Dr. Melanie Campbell, for their invaluable feedback and guidance throughout my degree. Their insights and expertise have been instrumental in shaping my research and helping me achieve my academic goals.

Finally I would like to extend my thanks to Dr. Frank Wise at Cornell University and his students (both current and former) Pavel Sidorenko, Yi-Hao Chen, and Michael Buttolph for their help in working through this and for useful discussions through this progress, as well as sharing their code that I use in this thesis.

Table of Contents

List of Figures

List of Abbreviations

- ANDi - All Normal Dispersion
- CPA - Chirped Pulse Amplification
- CW - Continuous Wave
- FTL - Fourier Transform Limit
- GDD - Group Delay Dispersion
- GMMNLSE - Generalized Multi Mode NonLinear Schrödinger Equation
- GMNA - Gain Managed Nonlinear Amplification
- GNLSE - Generalized NonLinear Schrödinger Equation
- GVD - Group Velocity Disperion
- MRG - Multi-frequency Raman Generation
- NPE - Nonlinear Polarized Evolution
- PM - Polarization Maintaining
- SMF - Single Mode Fiber
- SPM - Self Phase Modulation

"Any man who afflicts the human race with ideas must be prepared to see them misunderstood."

- H.L. Mencken

Chapter 1

Introduction

Preamble

Over the last century, physics has seen tremendous advancements, and one of the most significant discoveries during this time is the invention of the laser. The laser, which is now a common term in the dictionary, is an acronym for light amplification by stimulated emission of radiation. This invention revolutionized the field of experimental nonlinear optics, which was first proposed to exist by Maria Göeppert Mayer during her PhD in 1931[13]. Her work on two-photon absorption laid the foundation for the study of nonlinear optics, which deals with the interactions between light and matter in materials that do not have a linear response to electromagnetic fields. The confirmation of Göeppert Mayer's theory was later experimentally demonstrated by Bell labs in 1961[21]. Since then, the laser has become a ubiquitous tool in modern science and technology. The laser's unique properties, such as its high degree of coherence, narrow bandwidth, and intense power, have enabled numerous applications in diverse fields, from manufacturing and telecommunications to medicine and entertainment.

In this thesis, we focus on fiber lasers, one of the many types of lasers that have emerged since the invention of the laser. Fiber lasers are highly attractive due to their low cost to build, their compact size, their efficiency, and their gained stability from the reduced need to align bulk free space components, as well as their reduced sensitivity to temperature and vibrations.

The main components of a fiber laser include a gain medium, an energy source, and a resonator. The gain medium is usually a fiber doped with rare earth elements, such as ytterbium (Yb) for our purposes. The energy source is typically a laser diode pump, which provides a continuous wave pump at a specific wavelength related to the absorption of the doped fiber. For Yb-doped fiber, the optimal pump wavelength is 976nm with a narrow bandwidth of about 1-2nm. Using pumps that are fiber output coupled is usually chosen to maintain high efficiency, although it is possible to couple the pump from free space to fiber. The final piece is the resonator, which allows the output of the fiber to couple back to the start of the fiber. This is a great place to add some free space components to the fiber laser, such as a method for the light to exit the cavity. Overall, fiber lasers have become an important tool for research and industrial applications due to their unique properties and advantages. In this thesis, we will explore the properties and performance of fiber lasers and their applications in nonlinear optics as well as in ultrafast optics.

Ultrafast optics is a rapidly advancing field of laser research that focuses on the generation, manipulation, and measurement of light pulses that are incredibly short in duration, typically on the order of femtoseconds up to a few picoseconds. The applications of ultrafast optics are widespread and diverse. For example, ultrafast lasers are used in materials science to study the properties of materials and chemicals with high temporal resolution[12, 7], which can help researchers understand the fundamental mechanisms that underlie chemical reactions, energy transfer, and light-matter interactions. In biology and medicine, ultrafast lasers are used to create highly precise cuts or ablations in biological tissue[11], making them valuable tools in medical diagnosis, surgery, and treatment. Furthermore, ultrafast optics has enabled the development of new technologies such as frequency combs, which provide a way to precisely measure the frequency of light and can be used for a wide range of applications including spectroscopy[32], optical clocks[16], and telecommunications[23]. The ability to generate and manipulate ultrafast light pulses has also paved the way for the development of ultrafast imaging techniques, which enable scientists to capture real-time images of fast-moving processes at the atomic and molecular scale[2]. Overall, ultrafast optics is an exciting and rapidly advancing field of study that has the potential to transform our understanding of the physical world and lead to new technological innovations in a wide range of fields.

1.1 Research Objectives

The main focus of this thesis is to investigate an ultrafast laser system comprising an all-normal dispersion (ANDi) fiber laser and a gain-managed nonlinear amplifier (GMNA). The goal of this research is to optimize the performance of the laser system for use in future research projects. To achieve this goal, two primary objectives have been identified.

The first objective of this thesis is to stabilize the mode-locking conditions of the ANDi fiber laser. Achieving stable mode-locking is crucial to reduce the time spent adjusting the system in order to achieve mode-locking. Currently this can take several weeks and can be lost within a few hours. By increasing the stability of the mode-locking, the laser will remain mode-locked for significantly longer periods, and should require less than 10 minutes to achieve a mode-locked state whenever the state is lost. The mode-locking state should also be stable enough that if the cavity is blocked so that the light can not oscillate for a few seconds the mode locked state should return without any intervention once unblocked.

The second objective is to explore the spectral broadening and amplification of the GMNA output using the ANDi as an input seed. This will be accomplished by experimentally monitoring the spectral changes while varying the seed power and pump power independently. The band-pass filter and half wave plate in the system will also be adjusted by the same standards to ensure the optimal spectrum for the seed and correct polarization is chosen to seed the amplifier, so that it should match the simulated spectrum for the corresponding pump and seed power. By examining the changes in the spectrum and the efficiency of the amplification, optimal conditions for using the amplifier can be chosen such that the spectrum is at minimum 100nm wide, but ideally made as broad as possible while also ensuring the efficiency of the laser is 40% or better.

In pursuing these objectives, this research will delve into various aspects of nonlinear optics, specifically related to this ultrafast laser system. Through this investigation, we aim to advance our understanding of ANDi fiber lasers and GMNA, leading to improved performance and increased efficiency for future research applications.

1.2 Structure of the Thesis

This thesis is structured into five chapters. Chapter 1 provides a comprehensive overview of the background theory necessary to understand ultrafast laser systems, including key concepts such as dispersion and nonlinear effects. Chapter 2 introduces the ANDi fiber laser, which forms the basis of the ultrafast laser system studied in this thesis. This chapter will cover the theory and design of the ANDi laser, including its physical components and operational principles, and the mode-locking state of the ANDi laser, exploring the factors that influence its stability and how to achieve sustained mode locking. In Chapter 3, the focus shifts to the GMNA, which amplifies the output of the ANDi laser. This chapter will introduce the theory and design of the GMNA, including a section on the compressor system necessary to match more optimal amplifier conditions. Chapter 4 presents the data as the main work of this thesis while also providing some analysis and interpretations of the data. This includes sections focusing on the stabilization of the mode-locking for the ANDi fiber laser and optimization of the GMNA output under varying pump and seed powers while evaluating changes in the spectrum and amplification efficiency. Finally, Chapter 5 summarizes the key findings of the thesis, highlighting their significance for future research projects.

1.3 Motivation

The research group has a great interest in the spectral broadening from a GMNA that is seeded by an ANDi fiber laser. In this thesis, the aim is to delve deeper into this system, to comprehend it better and use this knowledge to construct a two-color system later for two main projects our group works on. These projects are the multi-frequency Raman generation (MRG) and mid-infrared continuum generation.

To accomplish this, a two-color system with a specific frequency difference is required. Previously this was achieved in our lab through the use of a 65MHz repetition rate Yb fiber laser capable of delivering 200fs pulses with an average power of 400mW[37]. This laser seeded a all normal dispersion photonic crystal fiber to generate a continuum before a chirped fiber Bragg grating was used to create a notch in the center of the spectrum creating the two colors

at 1025nm and 1085nm. The two color seed average power generated was 28mW and required a chirped pulse amplifier (CPA) as a preamplifier in order to achieve 850mW average power. The addition of the preamplifier introduced gain narrowing in each color and is strongest below 1025nm. For the lab setup for this thesis we focus on seeding a GMNA using an ANDi fiber laser. The GMNA generates a broad spectrum from nonlinear effects to go beyond the gain narrowing limit which can be turned into a two color system by removing the center of the spectrum using notch filters and leaving a color on each side of the spectrum. Using this method we aim to generate a broader spectrum so that the separation of the two colors can be chosen such that they are further apart beyond the gain narrowing limit of the two CPA preamplifier, we also should achieve similar powers for the two color seed power without the need for a preamplifier. The goal of the spectrum must be at minimum broad enough at the end of the GMNA to achieve the desired frequency separation for the projects. The frequency separation of this system is expected to require that the two colors also be frequency doubled for the MRG project in order to achieve a difference of 23.25THz[15]. This frequency separation corresponds to the energy difference between the ground state and an excited state for SF_6 which will be the medium of choice for our group when studying MRG.

The ANDi fiber laser is a preferable choice over other near infrared lasers in these projects, mainly because it can produce ultrashort pulses on the order of a few picoseconds before compression, and if desired, can be compressed down to a few hundred femtoseconds. This makes it ideal for seeding a GMNA with relative ease, which is not as easily achieved from other near infrared lasers. Additionally, the majority of the laser is made up of optical fibers, which carries many benefits, such as being quite compact, avoiding the use of more complex elements such as chirped mirrors or grating pairs inside the cavity, the system can remain stable for long periods of time, and if built on its own, a small portion of an optical breadboard can be easily transported. The final advantage of the ANDi is that it can operate over a wider bandwidth compared to most near infrared lasers.

The GMNA system is preferred over the more traditional CPA system. In the CPA system, a laser pulse undergoes pulse stretching so that when the pulse has a much lower peak power, this allows for amplification that will avoid nonlinear effects such as self-focusing that will damage equipment. After amplification, the pulse will then have to be compressed back to an ultrafast

pulse. Since the CPA system doesn't broaden the spectrum, this would have to be achieved using another method after amplification, adding an extra stage to the system. The GMNA system makes use of controlled nonlinearities from an already ultrafast pulse to both amplify the pulse and broaden the spectrum. The broadening achieved should be around 100nm or more, but it will depend on the seed pulse. Since the GMNA is entirely fiber, it has a very simple and cheap design to build and reduces the total amount of parts in the system. Although it is worth mentioning that polarization maintaining (PM) fiber is used, so it will require a fiber splicer capable of making PM splices which on its own can be expensive to buy, but if you have access to one like I do this is not too much of a worry. Due to this being a simple fiber system, it has the added benefit of being highly efficient. Finally, a GMNA provides high-quality pulses that can be compressed to just a few tens of femtoseconds, which is much faster than what is achievable by the CPA system.

1.4 Background Theory

1.4.1 Generalized Nonlinear Schrödinger Equation

Nonlinear optics is a field of study that is concerned with the behavior of light in nonlinear media, where the interaction between light and matter is nonlinear. Nonlinear optics has many practical applications, including in laser systems, where it is used to generate ultrashort pulses and to control the properties of the laser output. The study of nonlinear optics in laser systems requires an understanding of the specific nonlinear effects that occur in these systems, which are described by mathematical models such as the generalized nonlinear Schrödinger equation (GNLSE). In this thesis, I focus on the nonlinear effects that occur in laser systems, particularly in the propagation of laser pulses. To describe these effects, we use the GNLSE, which is a widely accepted model for the electric field of laser pulses in optical fibers. The GNLSE includes both linear and nonlinear terms that account for various phenomena, including dispersion, self-steepening, Raman scattering, and the self phase modulation. These effects will be described individually in more detail in the following sections of the introduction portion of the thesis.

In our study, we use a specific version of the GNLSE called the generalized multi-mode

nonlinear Schrödinger equation (GMMNLSE) which is used for analytical and computational modeling of ultrafast pulse propagation in multi-mode fibers. This version of the GMMNLSE is used to computationally model both the ANDi fiber laser the GMNA, in which only a single fundamental mode is considered. The ANDi fiber laser can be directly evaluated by the GMMNLSE by assuming a constant gain profile, in contrast the GMNA requires solving gain rate equations which can then be inputted to the GMMNLSE to be solved. The code that uses these models for the ANDi and GMNA were provided to us by Cornell University.

The GMMNLSE and its analytical solution for the ANDi fiber laser in section 2.1. The analytical solution of the GMMNLSE is an important tool for understanding the behavior of laser pulses in optical fibers and for optimizing the design of laser systems. In addition to analytical solutions, we also use computational modeling to study the behavior of laser systems. Computational modeling allows us to simulate the behavior of laser systems under different conditions and to study the effects of different parameters on the laser output quickly. Overall, the GNLSE and its specific version, the GMMNLSE, are important tools for studying the nonlinear effects that occur in laser systems. By understanding these effects, we can optimize the design of laser systems for specific applications and improve their performance.

1.4.2 Dispersion

Dispersion is a phenomenon that occurs when different colors of light travel at different speeds through a medium, which leads to the distortion of the shape of a pulse. This effect is due to the frequency dependency of the refractive index of the material through which the light is propagating. In other words, the refractive index of the material varies with the frequency of light, causing the light of different frequencies to experience different levels of slowing down or speeding up as it passes through the material.

Dispersion can manifest in two ways: spatial and temporal. Spatial dispersion results in the divergence of the beam and the appearance of different colors of light in different locations. Temporal dispersion, on the other hand, leads to a broadening of the pulse duration as the different frequencies in the pulse arrive at different times. In the context of ultrafast optics, it is crucial to control dispersion because it can have a significant impact on the shape, duration,

and intensity of laser pulses.

To quantify dispersion, one can examine the phase change of a light wave as a function of its frequency, known as the phase-frequency relationship. This relationship is commonly represented as a Taylor expansion, where the phase change is expressed as a series of derivatives with respect to frequency. The first term in this expansion is the absolute phase, which is a constant. The second term is the group velocity dispersion (GVD), which measures the variation in the group velocity of different frequencies of light. The third term is the group delay dispersion (GDD), which is the second derivative of the phase with respect to frequency and describes how the pulse duration changes with frequency. The fourth term is the third-order dispersion (TOD), which is the third derivative of the phase with respect to frequency and measures the curvature of the phase-frequency relationship. Higher-order dispersion terms can also exist, but they typically have smaller magnitudes and are less important in most cases.

$$\phi(\omega) = \phi_0 + \frac{\mathrm{d}\phi}{\mathrm{d}\omega}(\omega - \omega_0) + \frac{1}{2}\frac{\mathrm{d}^2\phi}{\mathrm{d}\omega^2}(\omega - \omega_0)^2 + \frac{1}{6}\frac{\mathrm{d}^3\phi}{\mathrm{d}\omega^3}(\omega - \omega_0)^3 + ... \tag{1.1}$$

The behavior and shape of a pulse can be affected by these dispersion terms. For example, GDD can cause the pulse to broaden or compress in time, while TOD can introduce chirp, which is a frequency-dependent phase shift that changes the relative timing of different colors in the pulse.

Dispersion can be characterized by the propagation constant β and its derivatives β_n with respect to frequency and are material dependent. These constants can be used computationally, as is the case in many models for laser propagation in optical fibers, such as the models used to study the ANDi and GMNA systems. Dispersion can also be classified as normal or anomalous, depending on the sign of the second derivative of the wave vector with respect to frequency. If this value is negative, the dispersion is considered normal, and if it is positive, the dispersion is considered anomalous.

1.4.3 Self Phase Modulation

Self-phase modulation (SPM) is induced by a nonlinear optical effect called the Kerr effect that causes an interaction between an intense optical pulse and a medium with a refractive index that varies with the pulse intensity. When an optical pulse propagates through a medium with a varying refractive index, the pulse experiences a nonlinear phase shift, which causes the pulse spectrum to broaden. This phase shift is SPM.

To understand SPM, we can start with the electric field of an optical pulse propagating in a medium, which is characterized by its refractive index $n(t)$ and intensity $I(t)$. As the pulse propagates through the medium, it instantly responds to its own intensity change and induces a nonlinear phase change $\Phi_{NL}(t)$. The induced nonlinear phase shift can be described by the equation $\Phi_{NL}(t) = -n_2 I(t)\omega_0 L/c$, where n_2 is the nonlinear refractive index coefficient, ω_0 is the carrier frequency of the pulse, L is the length of the medium, and c is the speed of light in vacuum. The nonlinear phase shift causes the pulse to experience a broadening of its spectrum, which can be represented in the energy spectrum.

$$S(\omega) = \left| \int_{\infty}^{\infty} \tilde{A}(t) e^{-i\omega_0 t - i\Phi_{NL}(t)} e^{i\omega t} \mathrm{d}t \right|^2 \tag{1.2}$$

The instantaneous frequency and the variation of the instantaneous frequency of the pulse can be described by $\omega(t) = \omega_0 + \delta\omega(t)$ and $\delta\omega(t) = \frac{\mathrm{d}}{\mathrm{d}t}\Phi_{NL}(t)$, respectively. The largest change in frequency is approximately equal to the largest nonlinear phase shift divided by the pulse duration τ_0. The maximum nonlinear phase shift can be estimated by $\Phi_{NL}^{\max} \simeq n_2 \frac{\omega_0}{c} I_0 L$, where, I_0 is the initial amplitude of the pulse. If the maximum nonlinear phase shift is greater than 2π, the pulse experiences significant spectral broadening. Therefore, inducing a large nonlinear phase shift is critical to achieving the greatest possible spectral broadening.

When the nonlinear phase shift is large, it can exhibit an oscillatory structure in the frequency domain[1]. Specifically, the oscillations in the nonlinear phase shift are a result of interference between the pulse and itself caused by different parts of the pulse experiencing different phase delays as the pulse propagates in the medium. This is often very pronounced

at the edges of the spectrum for smooth roughly Gaussian pulse duration since the phase will depend on instantaneous intensity and gives large peaks on the edges of the spectrum but the exact shape of SPM is harder to predict analytically because it depends on many factors.

1.4.4 Raman Scattering

Stimulated Raman scattering is a third-order nonlinear effect that can be explained in terms of the energy levels of a material. In the quantum picture, Raman scattering occurs when two photons with frequencies ω_1 and ω_2 stimulate a medium, such as the doped optical fibers used in telecommunications (in our case, we consider the Yb-doped fibers). These two photons act to stimulate the medium from its ground state to a virtual energy level of energy $\hbar\omega_1$.

Once the medium is at this virtual energy level, it falls back down to an excited energy level of the medium with an energy difference of $\hbar\omega_2$. This means that the medium is now at an energy level of $\hbar(\omega_1 - \omega_2) = \hbar\omega_R$, where the frequency corresponding to the difference between the ground state and the excited state is called the Rabi transition frequency (ω_R). This process is known as Stokes Raman scattering and is shown on the left side of figure 1.1.

After the medium is in an excited state, it can be stimulated again by a photon with frequency ω_1, which causes the medium to be raised to a new virtual state. The medium then releases a photon of frequency $\omega_1 + \omega_R$ in order to fall back to the ground state. This process is known as anti-Stokes Raman scattering and is shown on the right side of figure 1.1. The Raman effect is an important phenomenon in fiber amplifiers since the intensity of the light is often strong enough to cause Raman scattering and will be discussed in the gain managed nonlinear amplifier theory section.

1.4.5 Nonlinear Polarization Evolution Mode-Locking

Pulsed lasers have found widespread use in many fields due to their ability to deliver high peak powers in short bursts. In applications such as material processing, laser micromachining, and laser spectroscopy, these high peak powers can enable new scientific discoveries and industrial processes. One important characteristic of pulsed lasers is the pulse duration, which can range

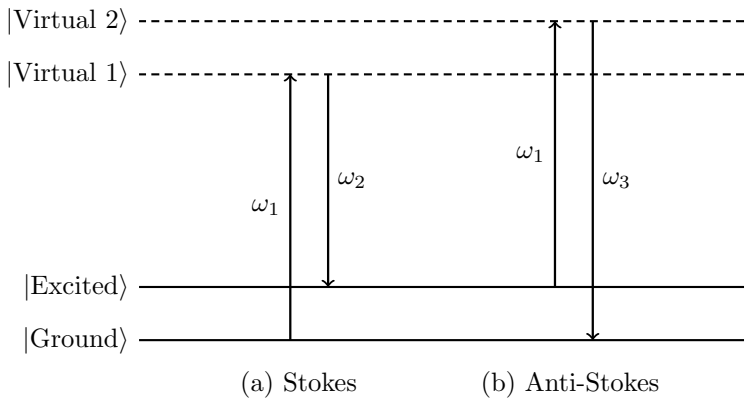

Figure 1.1: Here we can see pictures the quantum energy levels for both Stokes (a) and Anti-Stokes (b) Raman scattering.

from a few femtoseconds to several nanoseconds. The shorter the pulse duration, the higher the peak power and the more precise the laser can be in its application. Thus, there has been a strong research focus on developing high pulse energy and ultrashort pulse lasers.

One of the most effective methods for generating ultra-short pulses is through a process called mode locking, which produces a stable train of ultra-short pulses. Mode locking can be achieved through active or passive methods, where passive mode locking is particularly attractive due to its simplicity and reliability. Nonlinear polarization evolution (NPE) is a popular method for passive mode locking of fiber lasers. The NPE method makes use of nonlinear effects in the fiber, with the Kerr effect being the most important factor in the process. It's worth noting that while NPE is an effective method for producing ultra-short pulses, the pulses would still need to be compressed outside the oscillator if even shorter pulses are desired. Nonetheless, the advantages of NPE make it an attractive option for generating stable trains of ultra-short pulses for a variety of applications.

The key to achieving mode locking with NPE is to ensure that the laser cavity has a net normal dispersion[14]. This can be done by using a combination of positive and negative dispersion elements in the cavity, such as fiber Bragg gratings or chirped mirrors. As the name would suggest the all normal dispersion fiber laser has a net normal dispersion fiber cavity. When the laser is initially turned on, it operates in a CW state where the polarization of light in the fiber is in an elliptical state that evolves as it travels through the fiber due to random birefringence. By adding polarization controls, such as wave plates, an artificial saturable absorber is created. This allows for high transmission at the peak intensity where

the nonlinear effect is strongest. This CW signal contains a small amount of noise caused by quantum fluctuations[25]. Eventually one of these fluctuations will be large enough to cause a significant difference in the artificial saturable absorber based on the amount of Kerr effect it will experience and have a higher transmission then the CW signal, by oscillating this quantum noise a pulsed signal is generated over roughly 1ms. The NPE acts to shape the pulse as it evolves from noise but is not strong enough on its own and so additional pulse shaping techniques are needed and so a spectral filter is introduced to the system.

Spectral filtering can effectively aid in achieving mode locking in a cavity. This technique allows only a specific range of wavelengths, corresponding to the desired mode, to oscillate inside the cavity, while limiting those associated with undesired modes. It has several benefits, including stabilizing frequency against environmental drift caused by temperature change or vibrations, aiding in pulse shaping when noise is being selected as a means for self-starting mode locking, and eliminating noise from amplified spontaneous emission. It should be noted that a specific selection of center wavelength and bandwidth is required to achieve these benefits.

To achieve spectral filtering, a band-pass filter can easily be added. This filter permits a certain bandwidth at a center frequency to pass through while reflecting all other frequencies. The angle of the band-pass can be adjusted to change the center wavelength within certain limits. However, using a band-pass filter can be problematic because it requires custom design based on the desired bandwidth and center frequency.

Alternatively, spectral filtering can be achieved by using a single grating before a fiber. Instead of a mirror, the grating can be placed to align the seed back into the fiber. This approach offers a more flexible and convenient way to achieve spectral filtering because it doesn't require custom filter designs. By adjusting the distance between the fiber and grating, the bandwidth of the filter can be controlled, while the center wavelength can be tuned by varying the angle of the grating. This type of filtering can be seen in figure 1.2.

1.4.6 Experimental Techniques and Equipment

This thesis employs several optical techniques, which require an explanation of their workings. An autocorrelator will be used to measure the pulse duration of the laser and amplifier outputs,

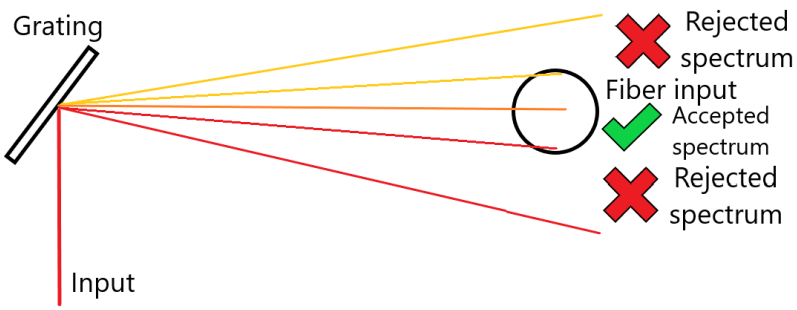

Figure 1.2: Here a reflective grating separates a beam into a line that varies by wavelength across a 2D line. Part of this line is aligned to go into the fiber and part of the spectrum is eliminated since it missed the fiber.

and a 2-grating pulse compressor system will be used to compress the pulse duration. It is essential to understand these tools.

In addition to these techniques, simpler equipment, such as a photodiode connected to an oscilloscope, will be used to show the light intensity over time of the laser. The photodiode is placed to measure a pick-off beam from the laser, which is introduced either by a beam splitter that sends only a small amount of power away from the main beam to measure the signal, or by finding a beam that is already being picked off and would otherwise be an inefficiency in the system. The intensity profile over a large time scale enables the measurement and observation of the laser's repetition rate, although it does not have a fast enough response time to measure the pulse duration itself.

Another piece of equipment is a spectrometer, which can take the output of any part of the system that is in free space and measure the intensity spectrum. This is necessary to check the proper mode locking conditions for the ANDi, as well as to measure and make changes to the spectral broadening of the GMNA.

1.4.6.1 Auto correlation

$$I(\tau) = \int_{\infty}^{\infty} I(t)I(t-\tau)\mathrm{d}t \tag{1.3}$$

Laser autocorrelation is a fundamental tool for measuring the pulse duration of a laser.

Measuring a pulse duration is an important method of evaluating the quality of a pulse, it is also extremely important when considering nonlinear effects since two pulses with equal pulse energies but different pulse durations have different peak powers. The intensity auto correlation method is based on equation 1.3 and is a particularly effective technique for measuring a pulse duration in the femtosecond to picosecond range, as it utilizes cross phase modulation to compare a pulse with a time-lagged version of itself.

The process of measuring the autocorrelation involves using a Michelson interferometer to split a laser beam into two paths. One of these paths is reflected off a mirror and directed back toward the interferometer, while the other path is transmitted through a second mirror and recombines with the reflected path at the output of the interferometer. By adjusting the length of the path traveled by the reflected beam, a time lag is introduced that allows the pulse to be compared with a delayed version of itself. You can see the schematic of an autocorrelator in figure 1.3.

The process of comparing the two pulses relies on cross phase modulation, which occurs when two beams of light interact in a nonlinear medium. When the two beams are focused onto the same spot of a nonlinear crystal, they produce a third beam with a frequency equal to the difference between the frequencies of the two input beams. This process results in a modulation of the phase of the pulse, which can be measured by comparing the pulse before and after the interaction with the nonlinear medium. To measure the cross phase modulation beam, an iris is used to block all of the beams except for the beam generated by the interaction of the two input beams in the nonlinear crystal. This will be the center beam out of the three and the output power of this beam is then measured using a power meter. The position of the iris and the power meter can be optimized by blocking each beam one at a time and adjusting their position until the power meter is only measuring the cross phase modulation beam.

Once the power of the cross phase modulation beam has been obtained, the autocorrelation can be calculated using equation 1.3. However, to obtain the original pulse shape from the autocorrelation data, a correction factor must be applied. This factor is dependent on the shape of the original pulse and can be calculated analytically. For example, for a Gaussian pulse, the correction factor is approximately 0.714, while for a sech-squared pulse, the correction factor is approximately 0.65. To confirm that the autocorrelation data has been correctly transformed

back into the original pulse shape, the process can be reversed, and the pulse can be re-autocorrelated numerically. If the resulting autocorrelation data matches the original data, the transformation has been successful.

In addition to the technical aspects of the measurement process, there are also a number of practical considerations that must be taken into account when performing an intensity autocorrelation measurement. For example, the quality of the nonlinear crystal used in the measurement can have a significant impact on the accuracy of the results, as can the stability and alignment of the interferometer. Furthermore, there are a number of different approaches that can be used to optimize the measurement process, including adjusting the pulse energy and optimizing the polarization of the input beams.

Overall, intensity autocorrelation based on laser autocorrelation is a powerful and flexible technique for measuring pulse duration in the femtosecond to picosecond range. With careful optimization and attention to detail, this method can provide accurate and reliable measurements of pulse duration.

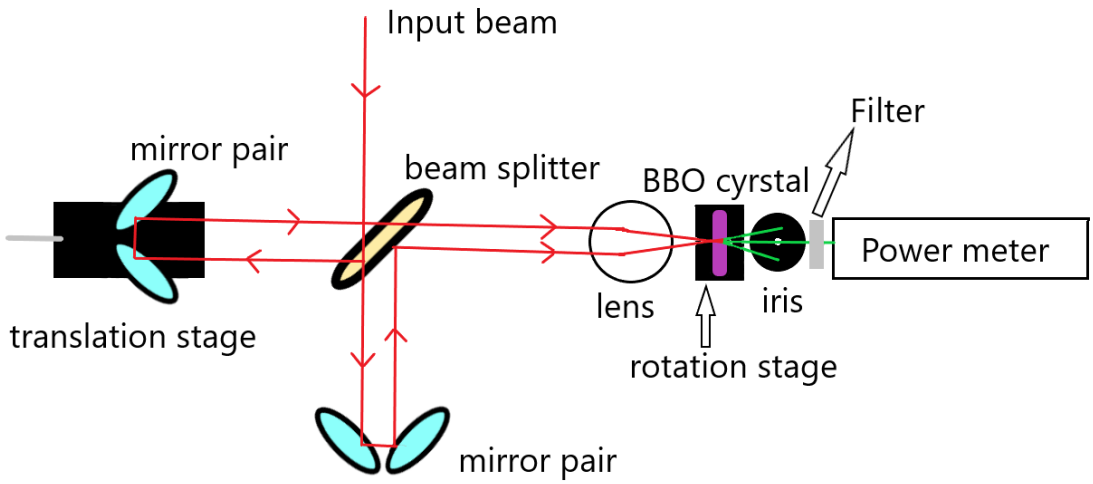

Figure 1.3: Schematic of the autocorrelator that will be used to measure pulse duration.

1.4.6.2 Pulse Compression

Pulse compression is an essential technique to reduce the temporal duration of stretched out pulses caused by dispersion effects. The use of prisms and gratings is a common method to control dispersion, however, the compressed pulse duration is limited by the Fourier transform

limit. The Fourier transform limit (FTL), also known as the uncertainty principle of the Fourier transform, is a fundamental principle in signal processing and applied mathematics that relates to the trade-off between the time and frequency domains of a signal. In essence, the FTL states that it is impossible to obtain simultaneous perfect resolution in both the time and frequency domains of a signal. Specifically, if a signal is narrow in the time domain, then its frequency spectrum will be broad, and vice versa. Mathematically, the Fourier transform limit can be expressed as:

$$\Delta t \Delta f >= \frac{\pi}{2}$$

where Δt is the temporal duration of the signal, Δf is the frequency bandwidth of the signal. This inequality means that the product of the temporal duration and frequency bandwidth of a signal cannot be smaller than a certain value, which is $\frac{\pi}{2}$. This limit is also affected by the shape of the pulse duration and by using the half maximum full width bandwidth Gaussian pulses have a limit factor of approximately 0.44, while sech^2 shaped pulses have a limit factor of approximately 0.315.

A compressor system is typically built to correct temporal dispersion by utilizing spatial dispersion caused by gratings. By introducing a time delay, different frequencies travel slightly different path lengths throughout a round trip while both causing and correcting the spatial dispersion. A basic 2 transmission grating compressor system can be constructed, as shown in Figure 1.4. To utilize the grating properly, a half wave plate must be added at the start of the system, assuming that the light is already linearly polarized such that the polarization of the beam will match the direction of the grooves of the grating. The second grating must have the same angle relative to the initial input beam to the compressor. After the second grating, the different wavelengths will be parallel and will hit a mirror with a minor angle up or down so that the returning beam is separate from the input beam, alternatively a roof mirror could be used to offset the beam going into and out of the mirror. Going back through the second grating and then the initial grating will again cause a beam path difference between the different wavelengths. The distance separating the two gratings and the grating constants control how much the beam paths vary. As a result, the larger wavelength will have traveled a

greater distance than the shorter wavelength in our case later in the thesis, reducing the chirp of the pulse, as shown in Figure 1.4.

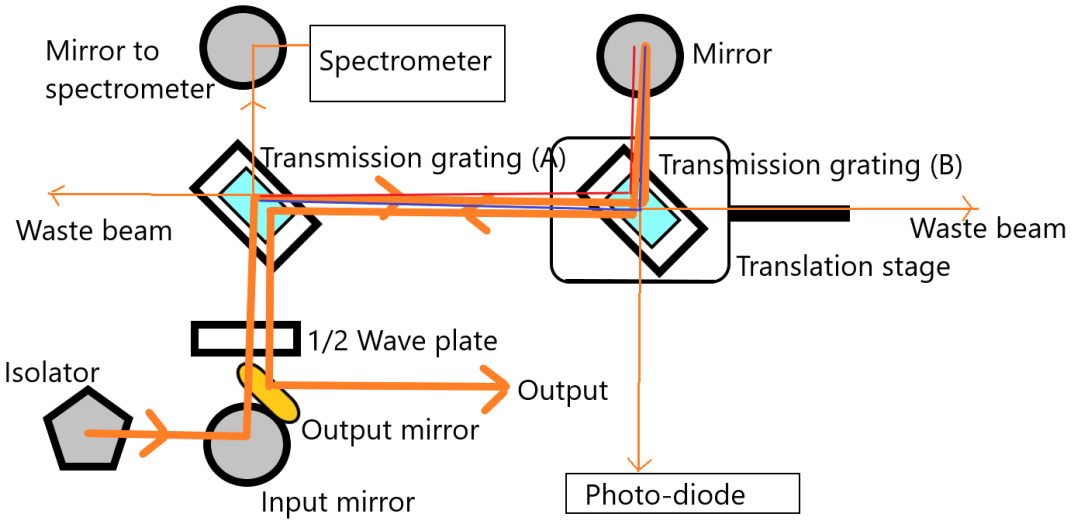

Figure 1.4: Schematic of two transmission grating compressor. In addition to the compressor there is also the beams shown for monitoring the mode locking state of the laser by using waste beams for the spectrometer and photo-diode

This type of compressor uses the following formulas below for the dispersion where c is the speed of light in a vacuum, L is the separation distance, θ_i is the incidence angle, d is the grating spacing, m is the diffraction order and λ is the wavelength. By calculating the GDD and TOD (given in equation 1.4 and 1.5) for the compressor and knowing the original pulse duration and shape, it can predict the distance the two gratings must be apart in order to achieve a specific compressed pulse duration up to its limit, although the actual limit of the pulse duration is often longer than the Fourier transform limit due to the fact that it is extremely difficult to achieve a perfectly linear spectral phase. Non-linear spectral phase can arise due to several factors, including the finite bandwidth of the gratings, imperfections in the grating structure, and deviations in the initial pulse duration and shape. To improve the likelihood of achieving compression down to the FTL, it is helpful to work with laser systems and amplifiers that produce pulses with an already roughly linear spectral phase. This reduces the impact of non-linearities introduced by the compressor, making it easier to achieve the desired pulse duration.

$$\mathrm{GDD} = -\frac{m^2\lambda^3 L}{\pi c^2 d^2}\left[1 - \left(-m\frac{\lambda}{d} - sin(\theta_i)\right)^2\right]^{-3/2} \tag{1.4}$$

$$\mathrm{TOD} = -\frac{3\lambda}{2\pi c}\frac{1 + \frac{\lambda}{d}sin(\theta_i) - sin^2(\theta_i)}{1 - \left(\frac{\lambda}{d} - sin(\theta_i)\right)^2} \cdot \mathrm{GDD} \tag{1.5}$$

Chapter 2

All Normal Dispersion Fiber Laser

2.1 Theory

The all normal dispersion (ANDi) fiber laser was designed by Dr. Frank Wise's group at Cornell University in 2006 as a way of producing a fiber laser that is very compact and can produce ultrashort pulses through NPE mode locking technique. The other benefits this system is that it is reasonably cheap to build and can produce a reasonable pulse energy in the 10's of nanojoules range, the spectrum is reasonably broad at about 10nm, and can be compressible to around 100fs pulse duration.

At the time, ultrashort fiber lasers focused on balancing the nonlinearity and dispersion in the fibers. Fiber lasers at the time could be made to produce pulses of 200fs duration with a pulse energy of 0.1nJ[22]. These fibers lasers had anomalous GVD and normal GVD segments because of this there had to be the introduction of prisms, gratings, chirped fiber Bragg gratings or chirped mirrors inside the cavity causing significant losses in the cavity in order to compensate for the dispersion. This is in contrast to the basic benefits of building a fiber laser which is a compact system with low loss and so there was a push to try and eliminate these in the design while still focusing on increased peak powers, increased pulse energies, and

decrease pulse duration. These lasers focused on self-similar pulses where Ilday et al.[20] showed theoretically that increased normal GVD was required to produce higher pulse energies. While still including components for dispersion controls inside the cavity the pulse energies were able to get up to 14nJ[4] by systematically increasing the normal GVD still in the self similar regime. Buckley et al. was able to extend this to a laser cavity with cavity net normal GVD with the help of a spectral filter to bias the cavity for even higher pulse energies to achieve a pulse duration of 55fs and pulse energies of 15nJ.

The next step in femtosecond fiber lasers was the desire to remove the dispersion controls inside the cavity. Chong et al. extended this idea of Buckley et al. in applying strong spectral filtering to a cavity with only normal dispersion they were able to produce pulses with a pulse duration of 170fs and pulse energies of 3nJ[10] with the first ANDi laser, these pulses remain highly chirped until compressed outside the cavity. Although this was a step backwards in terms of pulse energy and pulse duration, this opened the door to further explore an oscillator without the need to include dispersion controls inside the cavity. Chong et al. were guided by simulations and showed 3 regions of solutions based on the gain bandwidth. For a bandwidth of $\gtrapprox$ 30nm the pulses are parabolic and evolve like a self-similar laser, a bandwidth $\approx$ 10nm the pulses develop sharp peaks on both edges of the spectrum and finally for a bandwidth of less than 10nm the solutions do not converge. As we will see later these sharp edges in the spectrum are a key indicator when our ANDi is in a stable mode locked state as well as monitoring the pulses. Just a year later Chong et al. showed both experimentally and computational that these cavities have a broad range of working conditions by comparing a 25MHz version to a 12.5MHz system[8]. By adjusting the parameters of the laser such as cavity length, gain fiber length, spectral filtering bandwidth, and pump power the group was able to achieve a pulse duration of 165fs with pulse energies of 22nJ with a stable self-sustaining mode locked state. This is a significant improvement on previous pulse energies while maintaining a reasonable pulse duration. They were able to achieve higher energies but the state did not remain self-sustained. This makes note of the fact that at the lower repetition rate (12.5MHz) the laser was much more prone to a multi-pulsing state when the cavity is being over-driven by the pump. This is a trade off of having higher pulse energies at the lower repetition rate but the cavity being more prone to undesirable qualities for the mode locking state.

Up to this point in time there have only been experimental results aided by simulations of the cavity. In 2007, Renningar et al. showed the analytic solution to the cubic-quintic Ginzburg-Landau equation with terms for the Kerr effect, GVD, dissipative processes and a quintic saturable absorber term.

$$U_z = gU + (\frac{1}{\Omega} - i\frac{D}{2})U_{tt} + (\alpha + i\gamma)|U|^2U + \delta|U|^4U \tag{2.1}$$

$$U[t,z] = \sqrt{\frac{A}{\cosh t/\tau + B}} \exp -i\beta/2 \ln\cosh t/\tau + B + i\theta z \tag{2.2}$$

Where U is the electric field envelope, z is the propagation coordinate, t is the retarded time, D is the GVD, f is the net gain and loss, Ω is related to the filter bandwidth, α is the saturable absorber cubic term, δ is the saturable absorber quintic term, γ is the cubic refractive index nonlinearity of the medium and B is kept as a free parameter used to classify different pulse shapes. It should be noted that A, B, τ, and θ are real constants.

$$\alpha = \frac{\gamma(3\Delta + 4)}{D\Omega} \tag{2.3}$$

$$A = -\frac{2(B^2-1)\gamma(\Delta+2)}{BD\delta\Omega} \tag{2.4}$$

$$\tau^2 = -\frac{B^2\delta[D^2(\Delta-8)\Omega^2 + 12(\Delta-4)]}{24(B^2-1)\gamma^2\Omega(D^2\Omega^2+4)} \tag{2.5}$$

$$\beta = \frac{\Delta - 4}{D\Omega} \tag{2.6}$$

$$g = -\frac{6(B^2-1)\gamma^2(D^2\Omega^2+4)[-8(\Delta-4)/D^2\Omega^2 - \Delta + 6]}{B^2\delta[D^2(\Delta-8)\Omega^2 + 12(\Delta-4)]} \tag{2.7}$$

$$\theta = -\frac{2(B^2-1)\gamma^2(\Delta+2)}{B^2D\delta\Omega} \tag{2.8}$$

$$\Delta = \sqrt{3D^2\Omega^2 + 16} \tag{2.9}$$

This equation can used to describe many types of mode locked lasers and their solution for the ANDi is a dissipative temporal soliton[30]. The solutions covered a wide range of conditions for the cavity which have significantly different spectra and autocorrelations of the dechirped pulse. They showed the shapes of the spectrum can vary from a thin single narrow peak for

large values of ($B = 35$), to a flat spectrum with narrow width as you go towards $B = 1$ from the right side, on the left side of $B = 1$ the spectrum starts to appear more as a smooth double peaked spectrum with peaks on the edges of the spectrum and a dip in the middle, and finally as B approaches -1 the double peak spectrum becomes less smooth and shows fringes. It should also be noted there is no solutions for $B \leq -1$. Renningar et al.[30] then verified these analytic results of these 4 cases to experimental results.

2.2 Design

The ANDi fiber laser design at its core is very simple. The design is based on 4 different regions, with the last region connecting back the first region allowing the light to oscillate. These regions in order are the first single mode fiber(SMF) section, the gain fiber section, a second SMF section, and finally the nonlinear polarization evolution(NPE) section which are all further explained below in their own subsections. A schematic of the design is given in figure 2.1 as well as a real picture of the ANDi used is given in figure 2.2 where each component listed with the corresponding number. This design has been slowly tweaked for improvements from the initial design by Chong et al. in 2006, who based their design of the ANDi on the versions of femtosecond fiber lasers that included dispersion control.

2.2.1 First SMF Region

The first section of single-mode fiber comprises several components: a fiber collimator (B) (8), a fiber isolator (15), passive fiber (9), a fiber combiner (10), and a multi-mode fiber pump (11). Except for the multi-mode pump fiber and its corresponding fiber on the fiber combiner, all the fiber used here is simple Hi1060 fiber with a core diameter of 8μm and a cladding diameter of 125μ. The multi-mode pump fiber has a larger core diameter of 110μm and an outer cladding of 125μm. Using a larger diameter fiber for the pump input enables more efficient power delivery and ensures that the pump power reaches the outer cladding of the output fiber of the combiner.

The fiber collimator is a small lens attached to the end of a Hi1060 fiber. This lens is seeded with the result from the end of the last region (the NPE region). The fiber then connects to

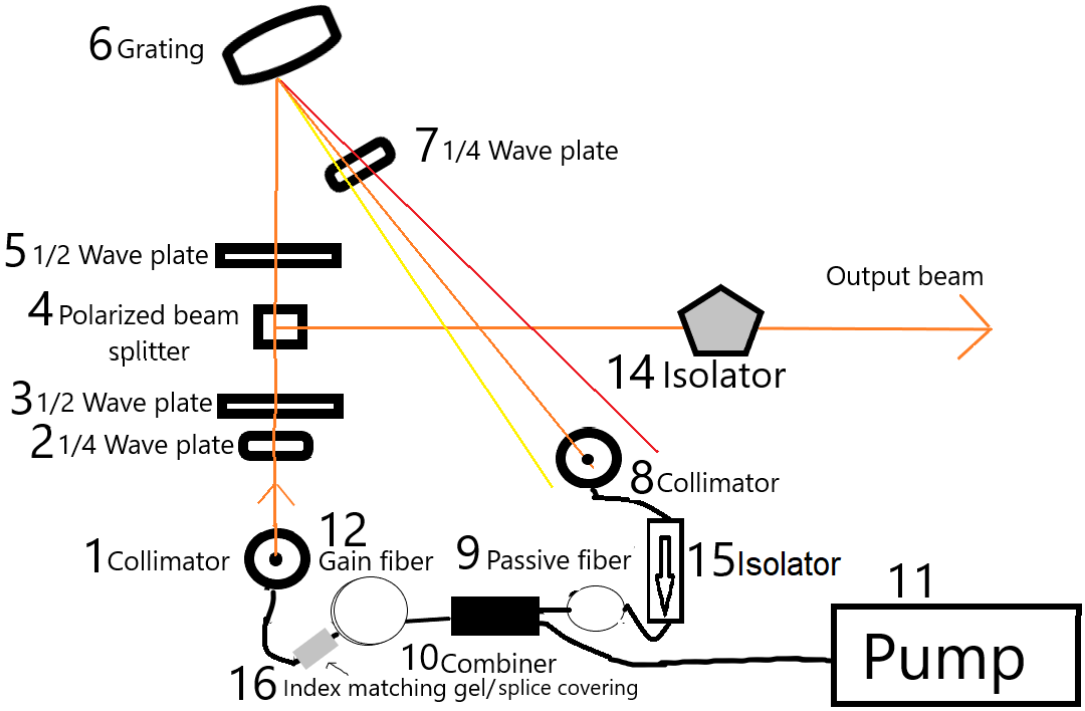

Figure 2.1: A schematic of the ANDi fiber laser used in lab.

1. Fiber collimator (A)
2. Quarter wave plate (A)
3. Half way plate (A)
4. Polarized beam splitter
5. Half way plate (B)
6. Grating
7. Quarter wave plate (B)
8. Fiber collimator (B)
9. Passive Fiber
10. Fiber combiner
11. Multi-mode fiber pump
12. Gain Fiber
13. Fiber holders
14. Free space isolator
15. Fiber isolator
16. Splice coverings (not pictured)

Figure 2.2: This figure shows the ANDi fiber laser in our lab with each component labeled in the image and corresponds to the diagram in figure 2.1

a fiber isolator that allows light to travel only in the direction towards the next region. Any additional single-mode fiber (SMF) added to the system to increase the cavity length of the laser follows the fiber isolator. It's worth noting that extending the fiber cavity will affect the repetition rate of the laser by increasing the round-trip time of the light.

The SMF fiber is then connected to the seed input fiber of the fiber combiner, which takes a second input from the multi-mode pump fiber. The combiner puts the input seed into the core of the output fiber while placing the pump in the outer cladding of the output fiber. The first SMF region ends at the end of the output fiber of the combiner. The length of fiber (excluding the pump fiber length) varies based on the desired cavity length but typically ranges between 6m and 15m. For this type of ANDi, these distances correspond to the upper and lower limit of the repetition rate. In this case, the length is very close to 15m.

2.2.2 Gain Fiber Region

This region is very straight forward. This solely consists of a short segment of gain fiber (12). For this particular ANDi a double cladded Yb doped fiber was chosen with an inner core diameter of 6μm and an outer cladding diameter of 125μm. This section of fiber is chosen based on the desired cavity length and is usually between 20cm and 50cm long. Yb fiber has high absorption at 976nm where it can efficiently be pumped to generate a pulse at 1030nm. The length of gain fiber needed can vary based on many factors such as the desired output power, the repetition rate of the laser, and the overall losses in the system.

When designing an ANDi you should start with a desired length of total fiber to know your repetition rate where you can use the approximation of Repetition rate = $\frac{L*n+d}{c}$. L is the length of all the fiber in the laser, n is the refractive index of silica fiber (≈ 1.5), d is the distance traveled in free space and c is the speed of light. From here you should use simulated results to determine an appropriate range of gain fiber. For a laser with 10MHz repetition rate the gain fiber should be around 0.5m long.

2.2.3 Second SMF Region

This region consists of a small segment of the SMF fiber attached to fiber collimator (A) (1), and the splice covering containing index matching gel (16). The first part of the region is the splicing point between the gain fiber region and this region, now that the beam is exiting the gain fiber we want to remove any leftover pump beam still inside the fiber. In order to keep the system in fiber as much as possible a gel is applied to the splicing point which matches the refractive index of the outer cladding of the fiber. Because the index is the same the pump light that is inside the fiber will leak out outside into the gel and be transmitted leaving only the seed in the fiber. The splice covering contains the gel and is used to absorb the power of the transmitted pump to prevent stray pump beams going off in any direction. After this it is simply traveling through the SMF until it hits the collimator that focuses the beam into free space for the final region. The total amount of fiber here should be roughly 1m or less but similar to the other regions can vary slightly based on the desired cavity length but this is less sensitive then the other regions.

2.2.4 NPE Region

The NPE region is entirely in free space and is made up of 2 quarter wave plates (2 and 7), 2 half wave plates (3 and 5), a polarized beam splitter (4), and a grating (6). As talked about in section 1.4.5 these polarizers act to control the polarization of the beam so that the output of the laser is taken from the polarized beam splitter which is the NPE ejection port. The beam coming out of the previous section has a nearly circular polarization and so the first part of the region is a quarter wave plate (2) to make the polarization linear. This is followed by a half wave plate (3) and polarized beam splitter (4) which controls the amount of transmission and reflection through the polarized beam splitter right after it. The reflected signal is the NPE rejection port and will contain the output beam which travels through a free space isolator (14) to prevent backwards reflections into the cavity. Continuing with the transmitted beam there is then an second half way plate (5) which is not required for NPE mode locking. This half wave plate is used before the grating (6) to ensure the linear axis of the light transmitting through the polarized beam splitter matches the grating axis. Figure 2.3

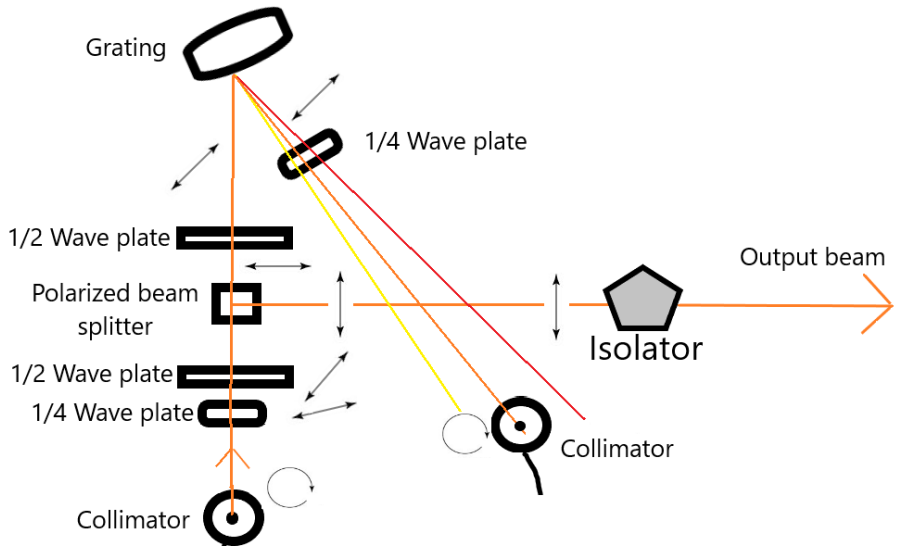

Figure 2.3: This figure shows the states of the polarization through the free space section of the cavity involved in the NPE region.

shows the states of the polarization through the free space section as they transverse through the difference components. The grating is added at this part for the spectral filtering. As mentioned in Chong et al. paper [10] there are many potential spots for the spectral filtering to be placed and it is not clear which spot is best theoretically. However practically this spot makes the most sense in terms of ease and simplicity of building the laser. Using a reflective grating we can simply place the final quarter wave plate (7) between the grating and the fiber collimator (B) (8) at the start of the first region allowing the light to be circular entering the fiber. By using this grating before the fiber only a small amount of the spectrum to enter the collimator causing spatial filtering. The extent of the spectral filtering is difficult to determine in this method but can be changed by varying the distance between the grating and the fiber collimator. By increasing the distance you decrease the amount of spectrum that can enter the fiber while bringing it closer will allow more of the spectrum to make it into the fiber. The distance of this section is mostly determined by the amount required for the chosen grating for spectral filtering but should be around 0.5m long and shouldn't be unnecessarily long.

2.3 Mode Locked State

The mode locked state of the laser is monitored through a photo-diode and spectrometer. As mentioned in the theory the spectrum of a mode locked state should appear as a double peaked

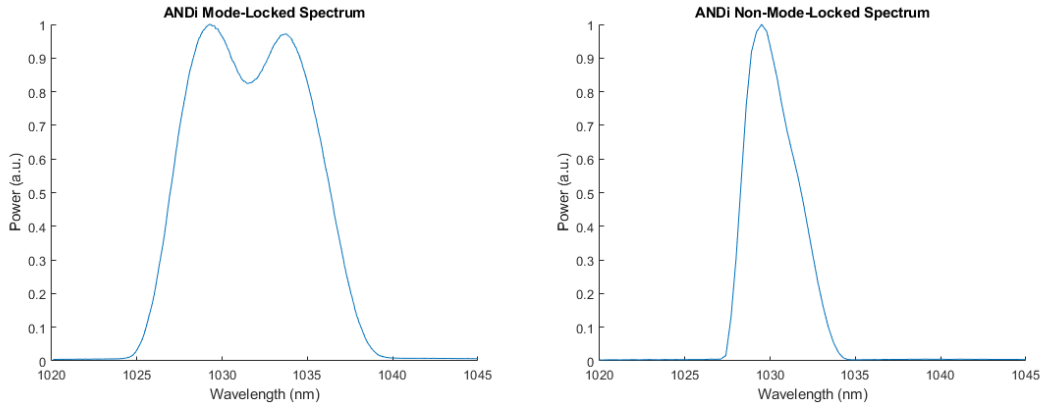

(a) (b)

Figure 2.4: The mode locked spectrum shows the double peaked structure caused by SPM shown in Renninger et al.[30] in (a) and in (b) we see the not mode locked (the continuous wave state).

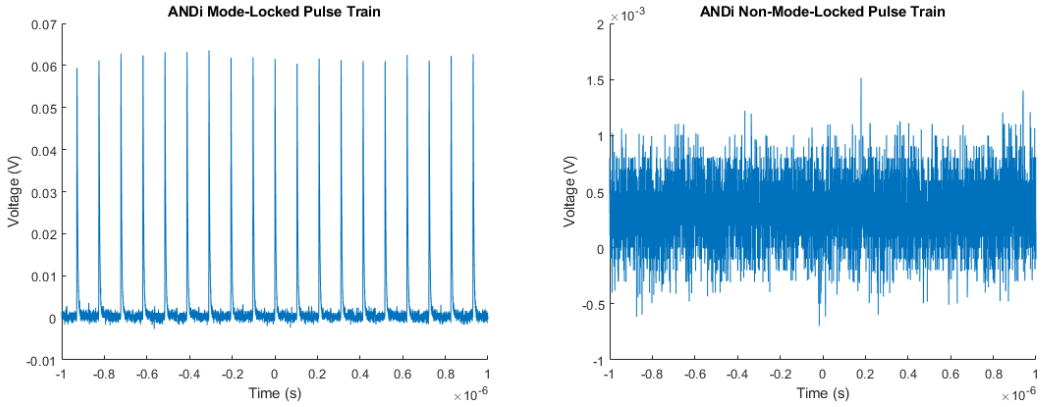

(a) (b)

Figure 2.5: This shows the mode locked pulse train taken from a photodiode connected to an oscilloscope with a repetition rate of 9.67MHz between pulses in (a). In (b) the photodiode is showing background noise of the continuous wave state.

structure for our laser. Figure 2.4 shows the difference between the non mode locked state and this mode locked structure which also exhibits a significant change in bandwidth of the spectrum. This transition happens discontinuously and is very easy to distinguish between while mode locking. However a spectrum is not significant to ensure the ANDi is in an acceptable state, a photodiode going to an oscilloscope is required to measure the pulses themselves coming from the ANDi. This is required because the laser can be in a multi-pulsing state but can be confirmed by having the correct frequency for the cavity length as well as roughly uniform amplitude between pulses. The following figures 2.4-2.5 show the difference between the two states as well as the mode locked repetition rate (9.67Mhz), center wavelength($1031nm$) and bandwidth(10nm).

Chapter 3

Gain Managed Nonlinear Amplifier

3.1 Theory

In the early years of research on nonlinear infrared laser fiber amplifiers, there were several challenges that had to be overcome. Two of the biggest challenges were achieving sufficient power output without damaging the fiber and balancing nonlinear effects appropriately for specific applications. One of the factors that were considered and optimized was through the use of different materials and doping techniques. For example, erbium-doped fibers were used to achieve amplification in the 1550 nm range, which is commonly used in telecommunications. There were also advances in the design and optimization of the amplifiers themselves. For example, new modeling techniques were developed that could predict the behavior of nonlinear infrared laser fiber amplifiers under different conditions. This allowed researchers to optimize the design of the amplifiers for specific applications. One of these designs is the gain managed nonlinear amplifier (GMNA).

The GMNA is a novel approach to nonlinear amplification that allows for leveraging the benefits of nonlinearities during amplification. It was designed by Dr. Frank Wise's group at Cornell University, who also developed the ANDi fiber laser. The GMNA operates in the gain

managed nonlinear regime, which is defined when the spectral broadening is balanced by gain shaping, resulting in a process of pulse evolution driven by a nonlinear attractor. This regime occurs in a relatively short co-pumped fiber (approximately 3m), where a narrow spectrum input seed (approximately 1-5nm) is inputted and results in a stretched output spectrum of 100nm or more, finally the central wavelength shifts to the red with higher pulse energies[33]. Being able to generate such a broad spectrum has great usage in making two color systems by removing the center of the spectrum.

The seeding conditions for the GMNA can be met by using an ANDi fiber laser and a band-pass or grating spectral filter technique to pick off one of the peaks of the ANDi spectrum, resulting in a pulse seed with a roughly Gaussian shape. However, it is important to note that the peak power must be in the right ranges to cause self-phase modulation (SPM) broadening while limiting other nonlinear effects. This peak power can be controlled through compressing or stretching the pulse duration of the input, matching the ideal conditions.

Before the use of the GMNA there were several different techniques such as direct amplification[39], pre-chirp management[27], and perhaps the most similar would be similariton amplifier[24], each had their drawbacks and benefits. The similariton similarly uses a nonlinear attractor, however suffers from worsening pulse quality when the bandwidth oh high energy pulses starts to exceed the gain bandwidth[36].

The GMNA was first shown experimentally and numerically to be able to give pulses up to 77nJ pulse energy and be compressible down to under 40fs[34]. Although this paper mostly focused on the results found for the amplifier under specific conditions, it was expanded later the same year to include much more detail about the pulses a GMNA could produce[33]. In this second paper, there was some very insightful discussion around the limit to which you can pump a GMNA. It was shown that there is a pumping threshold at which a sideband will appear to grow on the red side of the spectrum. This sideband was hypothesized to be generated from random noise, hence being incoherent and must be avoided, this was confirmed in the paper through numerical simulations involving a fixed amount of random photon noise at various wavelengths[33]. The same group again looked to push these limits to higher pulse energies by changing from a 10μm core Yb fiber to a 30μm core fiber. Due to the increase in effective area of the fiber, the nonlinear effects were significantly weaker at the same power in the fiber now

and so much stronger pumps and seeds could be used for much more powerful outputs. Doing this they were able to achieve 1μJ pulse energies again compressible to under 40fs. Overall gain managed nonlinear amplifiers are still a new area of research and much is still left to be known about them such as how to better control the gain shaping analytically and how they can be applied to more situations.

The computation modeling is done through solving the gain rate equations numerically using Runge-Kutta 4 in the interaction picture, the model of code was given to us by Dr. Wise's Cornell group and has had many contributions in building the code to where it is now [6, 5, 28, 19, 18]. Although the system is modeled as a multi-mode fiber, it only contains one significant mode (the fundamental mode), even though it is implemented in a large area mode fiber. This can be modeled for the number of modes as $n = 1$. These gain rate equations are as follows for a single mode fundamental mode,

$$\frac{\partial N_2(z,t)}{\partial t} = \sum_{k=1}^{K} \frac{\Gamma_k}{h\nu + kA_c}\left[\sigma_a(\nu_k)N_1(z,t)) - \sigma_e(\nu_k)N_2(z,t)\right]P_k^{\pm}(z,t) - \frac{N_2(z,t)}{\tau} \tag{3.1}$$

$$\frac{\partial P_k^{\pm}(z,t)}{\partial z} \pm \frac{1}{\nu_g(\nu_k)}\frac{\partial P_k^{\pm}(z,t)}{\partial t} = \pm\left[\Gamma_k\left[\sigma_e(\nu_k)N_2(z,t) - \sigma_a(\nu_k)N_1(z,t)\right]P_k^{\pm}(z,t) + \Gamma_k\sigma_e(\nu_k)N_2(z,t)2h\nu\Delta\nu\right] \tag{3.2}$$

where N_1 and N_2 are the populations of the ion density in the ground state and excited state respectively and where $N_T = N_1 + N_2$ is fixed, Γ_k is the geometric overlap factor, σ_a and σ_e are the absorption and emission cross sections, A_c is the core area of the fiber, τ is the lifetime of the upper excited state, $\Delta\nu$ is the frequency resolution, the $\pm$ factor represents the forwards $(+)$ or backwards $(-)$ propagation direction. The approach to this way of modeling in general was shown by Lindberg et al.[26].

Overall, the GMNA is a new area of research with much still to be learned, particularly in how to better control the gain shaping analytically and how it can be applied to more situations. However, the GMNA offers a promising approach to nonlinear amplification that can potentially be used in a variety of applications.

1. Input mirror
2. Half wave plate
3. Transmission grating (A)
4. Translation stage
5. Transmission grating (B)
6. Mirror
7. Mirror to spectrometer
8. Output mirror

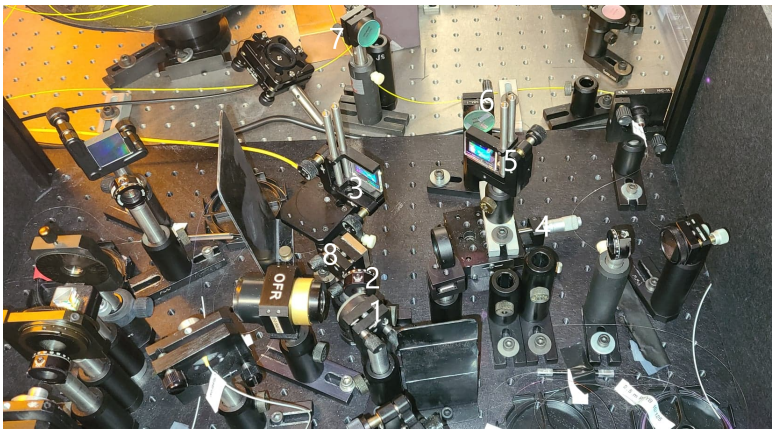

Figure 3.1: This figure shows the transmission grating compressor added between the ANDi and GMNA in order to compress the ANDi output to better match the pulse duration conditions of 0.5-1ps. It can also be seen that there is a photodiode and mirror taking some of the waist beams from the compressor in order to observe the mode locking of the ANDi.

3.2 Design

The pulse duration of our ANDi fiber laser is slightly longer than the ideal pulse duration for the desired spectral broadening of the GMNA in order to achieve the correct peak power to cause the SPM to broaden the pulse significantly. This is because the pulse duration coming directly out of the ANDi is 6ps with a repetition rate of roughly 10MHz while having roughly the same center wavelength (1030nm) and average power (50mW) compared to a previous version of this system. The previous ANDi had a repetition rate of close to 30MHz, a pulse duration of 0.5ps, and a estimated peak power of 3kW(assuming a Gaussian pulse shape, which would be expected from an ANDi). This difference in peak power is due to the changes in repetition rate and pulse duration of the laser and needs to be corrected to achieve proper spectral broadening due to SPM. Since the laser cavity is longer, proportionally the pulse duration lengthens. The pulse duration issue is resolved by adding a compressor before the amplifier. The basics of a 2 grating compressor is described in section 1.4.6.2. In figure 3.1 we can see the actual compressor in the system with the components labeled. The compressor is discussed in more detail in section 4.2.

The design of the GMNA is much easier to follow then the ANDi design. The GMNA is shown in figure 3.2 and consists of a free space region for spectral filtering and polarization control, a region of single mode polarization maintaining fiber (PM), and a region of gain fiber which is also PM. The hardest part of building this is the process of splicing PM fibers which

involves lining up the rods inside the fiber during the splicing. This splicing was done on a Vytran® filament fiber splicer for this purpose. A photo of the GMNA present in lab with various parts labeled can be found in figure 3.3.

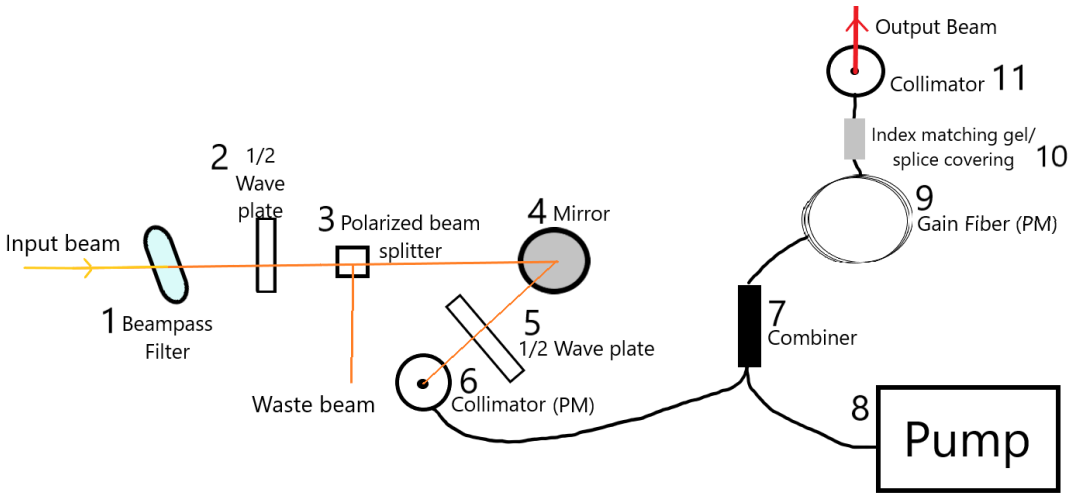

Figure 3.2: A schematic of the GMNA used in lab

1. Band-pass filter
2. Half wave plate (A) (post only)
3. Polarized beam splitter (post only)
4. Mirror
5. Half wave plate (B)
6. Fiber collimator (A)
7. Fiber combiner
8. Diode pump module
9. Gain fiber
10. Splice coverings
11. Fiber collimator (B)

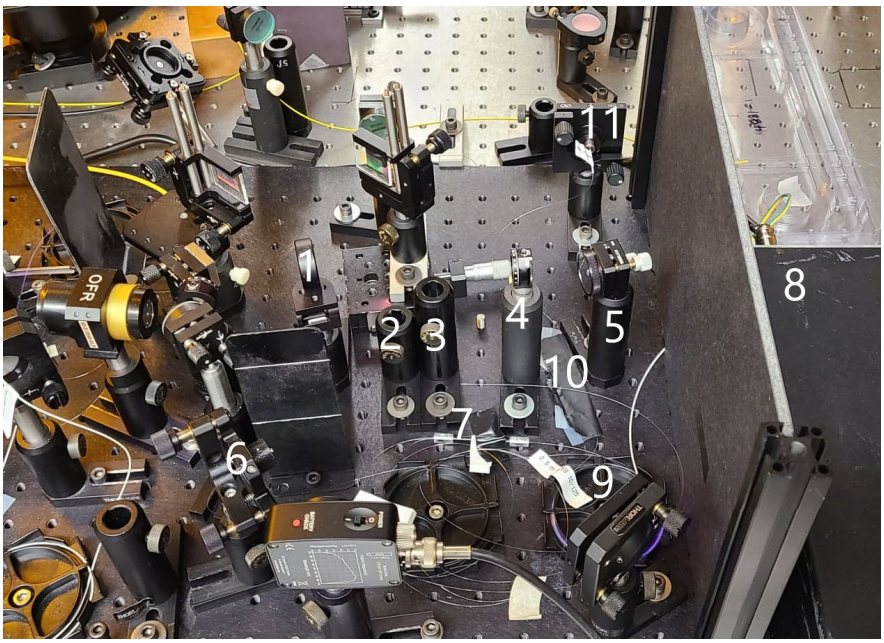

Figure 3.3: This figure shows the GMNA in our lab with each component labeled in the image and corresponds to the diagram in figure 3.2

3.2.1 Free Space Region

The free space region consists of multiple parts that control the seed input. From the output of the ANDi fiber laser the first part of this system is a transmission grating compressor. The ANDi requires 2 diagnostic detectors to ensure proper mode locking, these 2 detectors are placed so they can take some of the waist beams from the compressor. The schematic of the compressor is given earlier as well as an explanation in the introduction 1.4. The output of the compressor is then passed through a band-pass filter (1). This cuts the majority of the spectrum and power leaving only a small, roughly 4nm worth of bandwidth. The center wavelength is adjustable by adjusting the angle of the band-pass filter and can be used to optimize the spectral broadening of the GMNA. Then we place a half wave plate (A) (2) and a polarized beam splitter (3) after the band-pass filter. This acts as a saturable absorber by varying the power of the seed that will enter the amplifier. Following this is a mirror (4) used to align the beam into the fiber region and another half wave plate (B) (5) used to align the axis of polarization to match the polarization axis of the PM fiber.

3.2.2 PM SMF Region

This region of the GMNA is comprised of the input fiber collimator (A) (6) which is attached to a short piece of passive PM SMF, a fiber combiner (7), and a diode pump fiber (8). The collimator takes in the seed from the free space region and passes it as the input to the combiner and in a similar manner to the ANDi it puts this seed into the core of the output fiber while taking the multi-mode fiber from the pump as the pump input and putting this into the outer cladding of the output fiber. The output of this fiber is attached to the gain fiber section. The diode pump fiber is made of 105/125μm multi-mode fiber with an NA of 0.22 while the combiner input and output fibers are made of PM1060L-FA fiber with an NA of 0.06 to match the gain fiber and 105/125μm multi-mode fiber on the pump fibers to match the diode pump fiber.

3.2.3 Gain Fiber Section

The gain fiber section consists of a few meters of 10/125μm double clad PM Yb doped gain fiber (9). The length of the gain fiber depends more specifically on the input seed and is optimized through simulations for the seed but is typically around 2-3m long. The end of this is attached to a very short piece or roughly 15cm or less of matching passive PM SMF that is attached to a fiber collimator (B) (11) so the final output is in free space, this section of fiber should be as short so that there is no additional dispersion provided from the fiber. There should be an isolator following this part of the system to prevent reflection back into the amplifier, due to the broad spectrum a free space isolator is required since fiber isolator have smaller bandwidths. The splicing point between the gain fiber and the fiber collimator should be covered with index matching gel and a splice covering (10) to allow excess pump to leak through the fibers just like what is found after the gain fiber in the ANDi design.

In summary using a GMNA provides significant spectral broadening and amplification through nonlinear amplification that can be modeled computationally through the GMMNLSE and the gain rate equations. The GMNA has a simplistic design comprised of 3 main components, a free space region that allows the output from the ANDi fiber laser to be used as an appropriate seed, a passive fiber region that combines the seed and the pump, and a gain fiber region which is where the amplification takes place.

Chapter 4

Results

4.1 ANDi Mode-Locking Instability

The aim of this section is to investigate the stability issues the laser had experienced in our lab and make changes to improve the stability. The ANDi has trouble with both maintaining and achieving mode-locking. After many failed attempts at mode locking the laser by changing the polarization state of the free space cavity it was clear that changes to the system itself were required.

During the attempts to mode-lock the laser, it would show multi-pulsing where the pulses would happen twice as often as expected at varying amplitudes, this state is undesired for two reasons, maintaining this state for a long period of time can lead to damaging the fibers and this state is also not stable in the long term, as over time the extra pulses would drift from being equally spaced apart.

The first step in checking the lasers stability was ensuring that the cavity was properly aligned which was done by maximizing the output power by optimizing the input and output of the fibers. This yielded a CW beam of 60mW which roughly 20% higher then the pulsed output average power. For a 260mW pump this was exactly what is expected based on previous experience with ANDi lasers. This is also a great sign for the fibers themselves suggesting that there is no damage to them since efficiency was not an issue.

After checking the power optimization of the laser the next step was to attempt to achieve a mode locked state so that the spectrum could be analyzed even if this state was unstable or short-lived. Mode-locking is achieved by altering the polarizers slowly and careful while monitoring the spectrum from a spectrometer and a pulse train from a photodiode that is connected to an oscilloscope. The spectrum of the initially unstable mode locked state can be seen on the left in figure 4.1. The top is the experimental spectrum that was achieved and was roughly compared to a simulated ANDi with an estimate of the spectral filtering of 6nm to achieve the same type of spectrum. This simulated data was generated from code provided to me by members of Dr. Wise's group at Cornell University who have had several members contribute to the code over many years[5, 19, 28]. This code uses Runge-Kutta 4 in the interaction picture to solve the GMMNLSE to predict the behavior of the ANDi. The shape of the spectrum features two large peaks on the outside edges as would be expected in the ANDi theory although the presence of the additional structure in between the outer peaks suggests that this state is undergoing too much spectral filtering. This corresponds to being close to the $B = -1$ in the analytical theory in equation 2.2 and that the spectral filtering should be reduced (increase the allowed bandwidth) such that the solution is closer to $B = 1$ solutions. To make this change, the distance between the grating and input collimator was decreased, hence allowing more wavelengths into the fiber. Following this the system had to be aligned again for maximum output power and tested again. This greatly increased the stability of the mode locked state and resulted in the state of the right side of figure 4.1, again the top of the experimental spectrum achieved in the stable state while the bottom is the new simulated spectrum to match the experimental spectrum which required a spectral filter bandwidth of 10nm. By using the simulated spectra it helps to ameliorate the limitation that the amount of spectral filter inside the laser cavity is not easily measured directly when using a grating and fiber collimator to control the spectral filter. If instead a beam-pass filter was used you could use another half wave plate and polarized beam splitter to measure the amount of spectral filtering but this limits the ability to change the spectral filter bandwidth. Although there is a considerable change in how much power is in the center of the two peaks in the spectrum between the unstable and stable states it is more important to focus on the smoothness between the peaks than the amount of power.

There is one final adjustment that was made to ensure the best mode locking possible and

that is adjusting the x-axis alignment of the grating into the input collimator. This adjustment changes the center wavelength of the spectrum, in the unstable spectrum the only way to mode lock the laser at all was by centering the spectrum at 1040nm. From theoretical analysis it is indicated that the most stable center wavelength is 1030nm. As you can see in the stable spectrum the center wavelength is centered at 1032.5nm which is much closer to the ideal center wavelength. A limitation of taking these spectra is that the spectrometer I use does not provide the best resolution for a spectrum this small and that any structure seen in between the two peaks is hard to resolve.

With these changes, the ANDi now remains mode locked for months at a time and requires very little time to achieve a mode locking state when the state is lost. For example during a power outage, simply quickly turning the pump back on to the correct power instantly restored the laser cavity back into a mode locked state. The output of the ANDi is now 50mW, at a repetition rate of 9.68MHz.

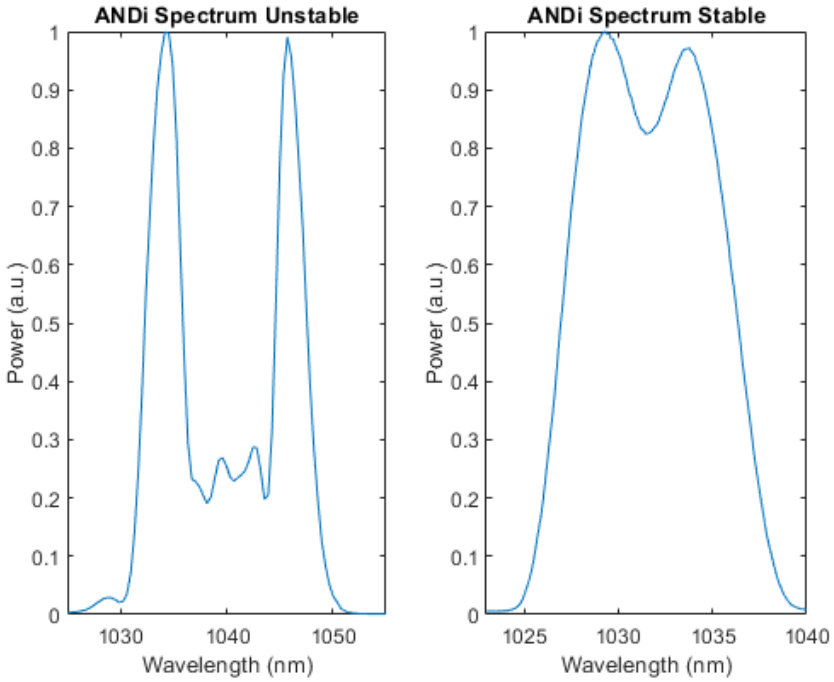

(a) Here we have the unstable mode locking spectrum that I started with from the ANDi on the left. It can be seen that there are more peaks in this spectrum between the two outer peaks, these extra smaller peaks can be referred to as additional structure in the spectrum. On the right side, is the new more stable mode locked spectrum showing just the peaks on the edges as expected although the middle of the spectrum is more filled in now.

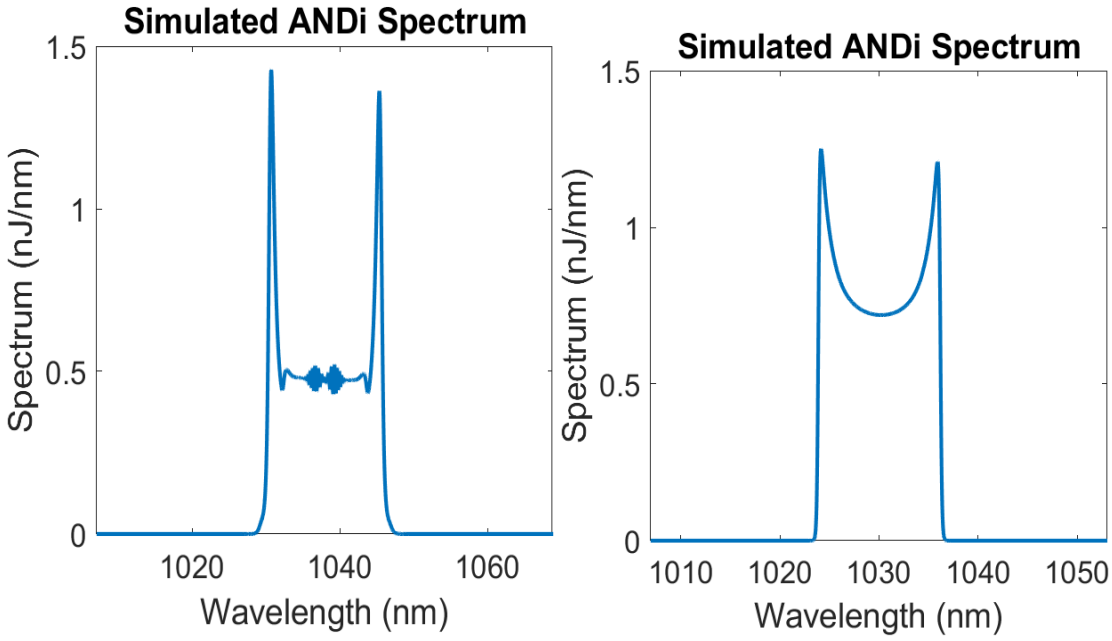

(b) This is the simulated spectrum produced by applying a 6nm bandwidth spectral filter centered at 1038nm, note the noisy middle between the outer peaks.

(c) This is the simulated spectrum produced with a 10nm bandwidth spectral filter centered at 1030nm, note the smoothness between the outer peaks.

Figure 4.1: A comparison between the experimental (a) results and the simulated results (b) and (c) that comes from changing the spectral filtering

4.2 GMNA Optimization

The final objective in the thesis is to optimize the GMNA spectral output by broadening the spectrum as much as possible while maintaining pulse quality. To start the optimization of the GMNA the system must be proceeded by a compressor system to achieve appropriate seed peak powers for nonlinear effects to occur. As mentioned earlier in the design section for the GMNA this is known through comparison with other systems that use a combination of an ANDi and GMNA. In the case of these other systems, the ANDi produces a pulse duration of a previous ANDi that has 50mW average power and is able to achieve large spectral broadening from the GMNA through a large nonlinear phase shift caused by SPM. That ANDi had a pulse duration between 0.5ps to 1ps at a repetition rate of 30MHz. Given that our ANDi outputs an average of just under 50mW power at the same wavelength it is reasonable to assume that our pulse duration needs to be shorter then 6ps to achieve the same peak powers, this is evident from any attempt to perform GMNA from the original seed since it only ever amplified the pulse without any broadening. The pulse shape remain constant between the different repetition rates and can be seen in figure 4.2 where the pulse durations were simulated and compared between a 12.5MHz and 25MHz ANDi. The pulse durations were chosen to match those used for comparing two ANDi lasers in Chong et al.[8], and are close to the repetition rates used between the two ANDi lasers I am comparing. These pulses were each able to achieve a similar pulse duration to that of Chong et al. after dechirping using a 2 grating compressor.

The compression for the seed was experimentally done through a two grating compressor shown in figure 1.4 where the distance between the gratings was adjusted via a translation stage under the second transmission grating to control the pulse duration in order to maximize the spectral broadening of the GMNA output.

The GMNA spectrum has many components that can be optimized to get the broadest spectrum possible. This broadening is often limited by the appearance of a red sideband. This type of sideband is generated by Raman scattering between the seed and random noise in the system, which is then amplified. Dr. Frank Wises group determined from simulations this was noise seeded by comparisons of the simulated amplifier to experimental results[33]. Since the sideband is generated by noise the light is incoherent and undesirable in a laser beam and

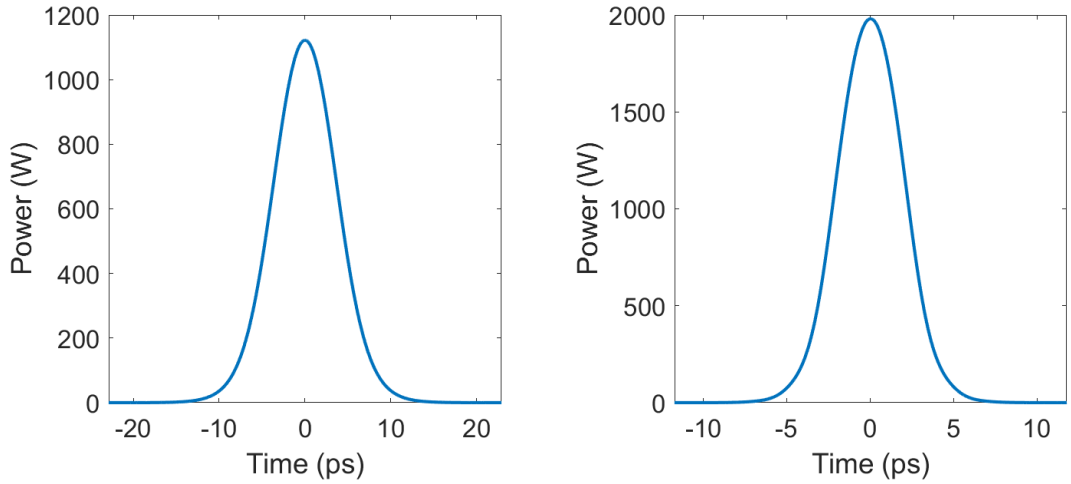

Figure 4.2: This figure compares the simulated pulse shape between the different repetition rates of ANDi at 12.5MHz (left) and 25MHz (right).

should be avoided as it can cause damage to the fiber as it gets amplified. The sideband is noticeable when the spectrum is plotted in the log scale as the shape of the spectrum will lose its sharp edges as the sideband quickly emerges. The PM nature of the fibers used in this system help to prevent noise such as amplified spontaneous emission, since the noise will have random polarization and so it will not effectively be amplified since most of the noise will not match the polarization axis of the fiber. I will now evaluate the factors of input seed power and the pump power on the broadening of the spectrum produced from the GMNA while watching for the appearance red sideband as an upper limit of the power.

While varying the system input power or pump power there are a few factors that need to be accounted for in the system to further maximize the spectrum. The axis of polarization should be fine tuned to match the axis of the fiber and can severely alter the broadening of the amplifier. This is controlled through the half-wave plate immediately before the input of the fiber since the incoming light is linearly polarized. The other factor is the band-pass filter which controls what part of the original spectrum coming from the ANDi and compressor is used for the input seed. This should be set to take one of the peaks of the ANDi spectrum since this will give the largest power while having a smooth approximately Gaussian spectrum as input. Finally, the alignment of the light into the input fiber is also crucial, as the input seed power can greatly affect the amount of spectral broadening. Therefore, it should also be adjusted whenever the band pass filter is adjusted. Since there is a small spatial chirp in the seed, as the beam-pass is rotated to allow different wavelengths, though the exact position of

the beam will also be altered and so this is adjusted for by re-aligning the final mirror before the input collimator to make sure the maximum input power and spectral broadening is still occurring.

To investigate the effect of input seed power on spectral broadening, I will place a half-wave plate and polarized beam splitter after the band-pass filter. This will allow me to control the amount power in the seed light by rotating the half wave plate to change the axis of polarization so when it hits the polarized beam splitter it will either pass through or go to being a waste beam. By looking at figure 4.3 you can see the spectrum broaden as the average power of the seed is increased. It should be noted the final power is taken when the half wave plate and polarized beam splitter are removed to allow the maximum amount of power present. Typically these would be left in the system to ensure the beam is linearly polarized, but with the addition of the grating compressor the beam is already linearly polarized and so this can be removed without affecting the polarization. The pump power is kept constant at 2W as this was found to be a pump power that avoided the appearance of a red sideband for all the seed powers.

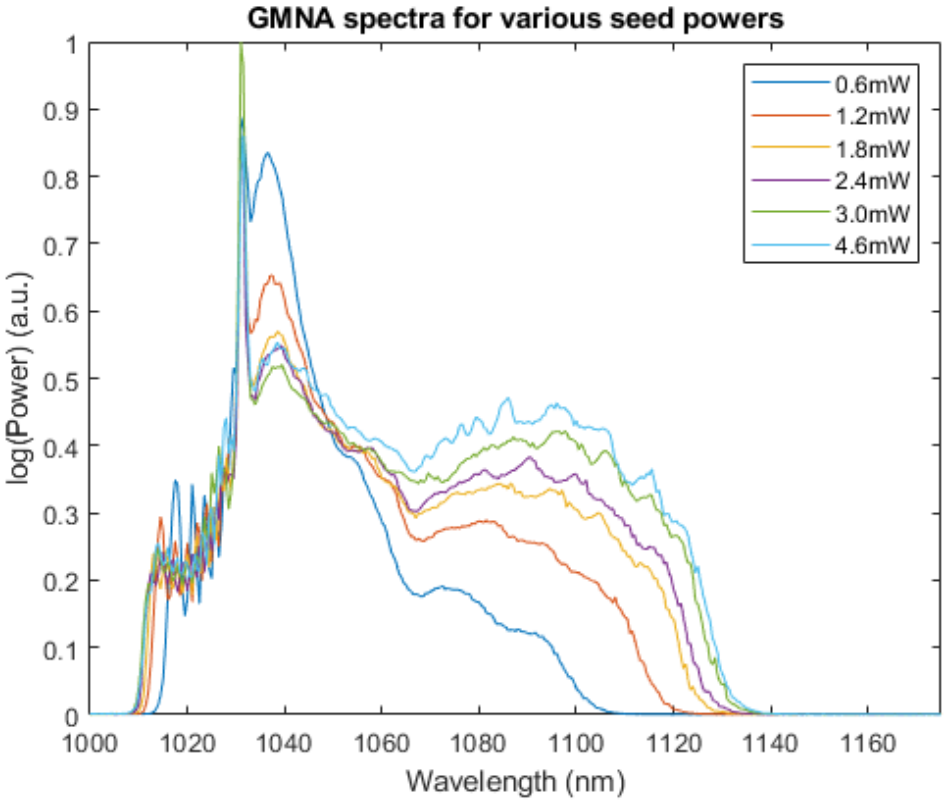

Figure 4.3: This shows the experimental difference in spectral broadening of the GMNA with various seed powers ranging from 0.6mW to 4.6mW. All seeds were amplified by a 2W pump power.

The presence of the sideband is examined in figure 4.4, where the log scale is used to determine it's presence. Since the long wavelength edge of the log scale spectrum drops off rapidly, no sideband is observed. The broadening has slowed down significantly as the big jump between seed powers of 3mW and 4.6mW show very little difference in broadening. There is a small difference though in the additional power in the longer wavelengths. The result is consistent with Sidorenko, Fu and Wise[33], who found that the spectrum shifts to the red side caused by a nonlinear attractor. By going below an average power of 0.6mW for the seed, there is no broadening at all and the seed is just amplified.

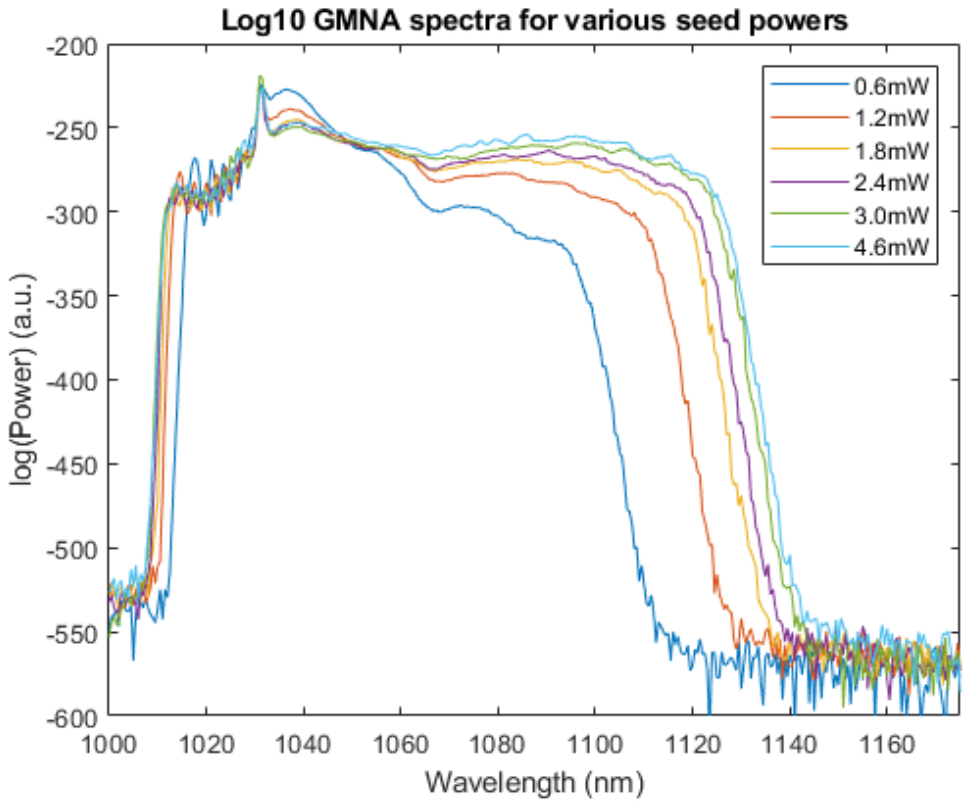

Figure 4.4: This shows the experimental difference in spectral broadening of the GMNA with various seed powers ranging from 0.6mW to 4.6mW in the log scale. All seeds were amplified by a 2W pump power.

I will now experimentally vary the pump powers for a maximum average seed power of 4.6mW. By changing the pump power, the spectrum will rapidly broaden, and as the power increases the presence of a red sideband will appear and start to grow, this is very evident in the log scale plot while being difficult to see in the linear plot. If the power is increased too quickly a sideband might be missed and thought to be rapid broadening caused by SPM instead of the red sideband. Figure 4.5 shows the linear plot of the spectra and figure 4.6 shows the log

scale for these spectra across several pump powers. At 4W pump the red sideband appears and is shown by the black arrow. At this point the sideband is tolerable to include in the spectrum since it makes up a very small fraction of the total power, if the system is required to be very insensitive to this noise operate the GMNA at a weaker pump power or use spectral filtering after the amplifier to remove the long wavelength edge of the spectrum. For pump powers in the log plot greater than 4W you can see that the red side of the spectrum is no longer a sharp drop off and is instead slowly decreasing.

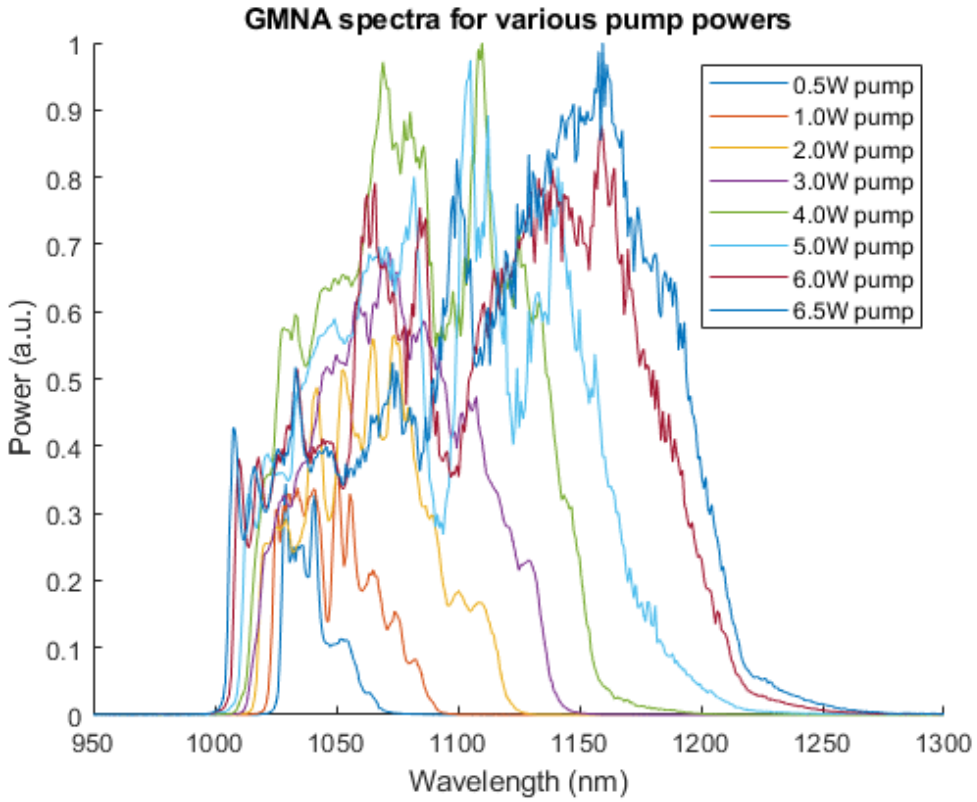

Figure 4.5: This shows the experimental difference pump power plays in the spectral broadening of the amplified seed. As you can see the higher the pump power, the more broadening that can be achieved. However this hits an upper limit around 4W pump power as suggested by the log plot in figure 4.6.

Experimental spectra for varying pump powers are compared to simulated results from modeling of the gain rate equations that then go into solving the GMMNLSE. To save space, these are shown in appendix A, where each pump power is plotted separately. The left plots are the linear spectra and the right plot is the log scale. Overall, there is great agreement between the simulated and experimental spectra, particularly at higher pump powers. The experimental results show more power on the blue side of the spectrum, likely due to some

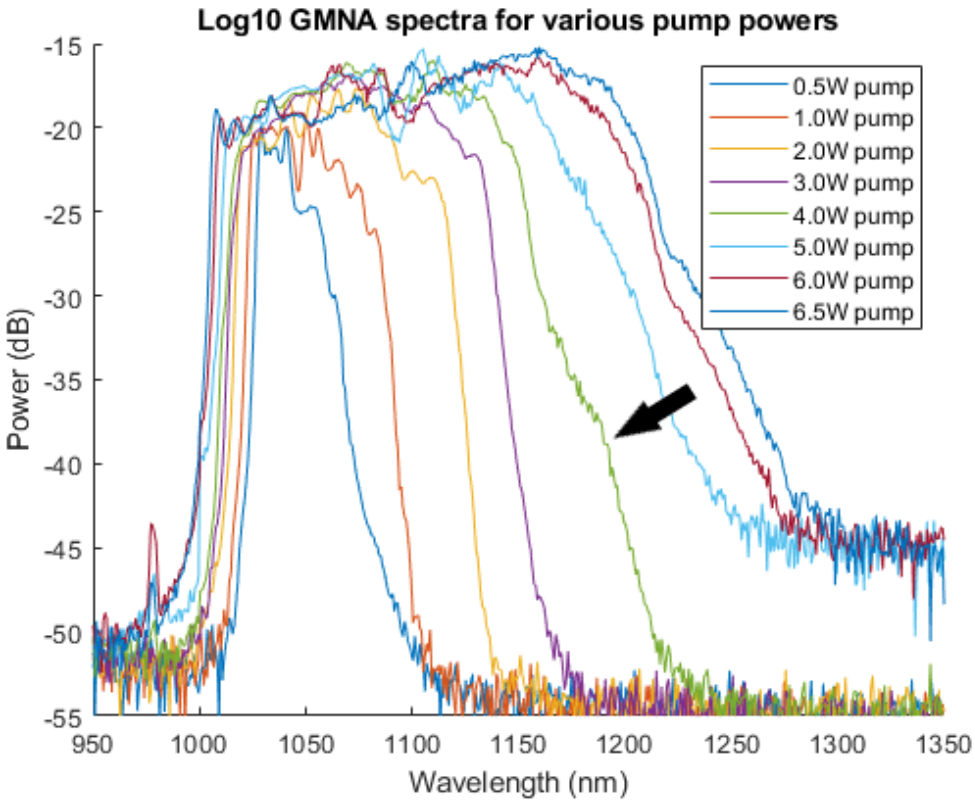

Figure 4.6: Here we can see the log scale of figure 4.5. The black arrow in the figure points to the start of the red sideband.

of the approximations of the initial seed conditions used in the simulation such as the pulse duration and shape, the input power and coupling efficiency, and initial chirp. The red sideband is more present at lower pump powers and is more separated from the main spectrum in the simulated spectra, likely because the value of 1000 photons per frequency bin in the simulation is higher then the actual amount of random noise in the system, but the value of 1000 photons per frequency bin was determined by Sidorenko et al. [33] to accurately model the GMNA and so it was kept consistent. It should be noted that very minor deviations in the half wave plate or beam pass filter will increase the presence of the sideband at lower pump powers similar to that of the simulation if care is not taken when aligning and rotating these components.

One important check for the amplifier is its efficiency, which is determined by a plot of output power verses pump power. The slope of this plot will give an efficiency for the amplifier. The plot may be nonlinear at very low pump powers but the plot overall should be linear. If the plot turns nonlinear after a linear region the amplifier is in a saturated state and a more powerful amplifier will need to be built to achieve higher powers. From figure 4.7 a best fit line

with slope of 0.442 fits the data and so the amplifier efficiency is 44.2%. The line remains linear over the whole range of data which means the amplifier is not experience saturation effects. This is great to see and can be used to ensure there is no damage to the amplifier.

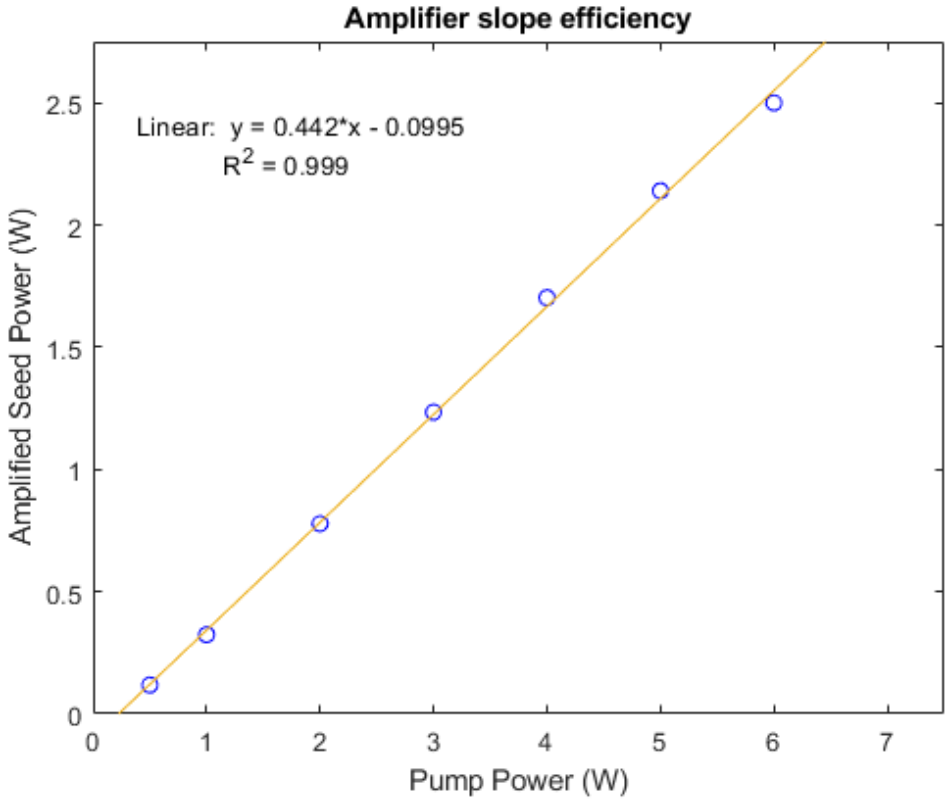

Figure 4.7: The slope efficiency of the GMNA. Best fit line shows $y = 0.442x - 0.0995$ with an $R^2 = 0.999$ Since this is still a linear relationship the amplifier is not saturated before getting into the noise seeded Raman regime.

Chapter 5

Conclusions

5.1 Summary of Results and Impact

The investigation of the stability issues with the ANDi laser showed that with decreased spectral filtering the laser was able to achieve stable mode-locking. The laser can now maintain a mode-locked state for months without any intervention, as well as being able to achieve mode locking when the power is turned off and back on. When the laser does stop mode-locking, it typically only takes minutes to bring it back into a mode-locked state. This has greatly reduced the amount of time wasted in lab in trying to achieve a pulsed mode-locked laser that can now be focused on other projects.

With the ANDi in a stable mode-locking state, the optimization of the GMNA spectral broadening was the next objective for this thesis. The GMNA has shown experimentally that a stable spectrum of over 100nm is achievable without the presence of a red sideband by pumping up to 4W while using the maximum power seed. The amplifier has an efficiency of 44.2% that remains unsaturated up to the point where red sidebands appear. The average output power at 4W pump is 1.7W, since The ANDi is pumping the amplifier with a repetition rate of 9.68MHz this yields a pulse energy of 176nJ. These experimental results closely matched the computational model for the GMNA as expected, together this shows us the compressor system worked great at being able to achieve significant spectral broadening.

This was the intended results for this thesis and the GMNA output is enough to use for the two color system where the spectrum will have the middle removed and then amplified again with the goal of broadening and smoothing the spectrum while also amplifying the beam again since a lot of energy is removed in the process of making the two colors. Since the spectrum at 4W pump power produces a spectrum that has a range from 1025nm to 1135nm, this will make an ideal notch in the middle be somewhere around 1050nm to 1110nm leaving a reasonable amount of power for both the short and long wavelength colors. This 60nm notch will provide the MRG project with the correct frequency separation once it is amplified again in a two color amplifier and then frequency doubled.

5.2 Future Research

The future research of this project related directly to a few projects going on inside our research group such as MRG, mid-infrared generation, and laser beat-wave acceleration. The MRG project is focused on achieving ultrafast pulses of a single femtosecond. The mid-infrared generation project aims to produce a laser source of significant power in the mid-infrared region also known as the fingerprint region. The first step in both of these projects is the development of a two color nonlinear amplifier built in a similar fashion to the GMNA.

Our lab group will attempt to build a fiber amplifier that makes use of nonlinear effects for a two color laser. The main goal of this second amplifier is to both amplify the two colors since a large portion of the power will be lost in the process of making the single broad spectrum of this system into 2 separate colors and be able to use nonlinear effects to further broaden the spectrum of each color. By broadening the spectrum we aim to overcome the gain narrowing found in the more standard two color CPA amplifier design. This research is driven by simulations solved the same way as the GMNA, by modeling the gain rate equations and then using them to solve the GMMNLSE. The simulated results will be taken and verified experimentally in lab. We are hopeful this design will overcome the disadvantages of the two color CPA system.

Bibliography

[1] Govind P Agrawal. "Nonlinear fiber optics". In: Springer, 2019.

[2] Irina Bocharova et al. "Charge resonance enhanced ionization of CO 2 probed by laser Coulomb explosion imaging". In: *Physical review letters* 107.6 (2011), p. 063201.

[3] Robert W. Boyd. *Nonlinear Optics, Third Edition*. 3rd. USA: Academic Press, Inc., 2008.

[4] JR Buckley et al. "Femtosecond fiber lasers with pulse energies above 10 nJ". In: *Optics letters* 30.14 (2005), pp. 1888–1890.

[5] Qianshun Chang, Erhui Jia, and W Sun. "Difference schemes for solving the generalized nonlinear Schrodinger equation". In: *Journal of Computational Physics* 148.2 (1999), pp. 397–415.

[6] Hung-Wen Chen et al. "Optimization of femtosecond Yb-doped fiber amplifiers for high-quality pulse compression". In: *Optics express* 20.27 (2012), pp. 28672–28682.

[7] Tae Y Choi, David J Hwang, and Costas P Grigoropoulos. "Ultrafast laser-induced crystallization of amorphous silicon films". In: *Optical engineering* 42.11 (2003), pp. 3383–3388.

[8] Andy Chong, William H Renninger, and Frank W Wise. "All-normal-dispersion femtosecond fiber laser with pulse energy above 20nJ". In: *Optics letters* 32.16 (2007), pp. 2408–2410.

[9] Andy Chong, William H Renninger, and Frank W Wise. "Environmentally stable all-normal-dispersion femtosecond fiber laser". In: *Optics letters* 33.10 (2008), pp. 1071–1073.

[10] Andy Chong et al. “All-normal-dispersion femtosecond fiber laser”. In: *Optics express* 14.21 (2006), pp. 10095–10100.

[11] Samuel H Chung and Eric Mazur. “Surgical applications of femtosecond lasers”. In: *Journal of biophotonics* 2.10 (2009), pp. 557–572.

[12] KJ Gaffney and Henry N Chapman. “Imaging atomic structure and dynamics with ultrafast X-ray scattering”. In: *science* 316.5830 (2007), pp. 1444–1448.

[13] Maria Goppert-Mayer. “Uber elementarakte mit zwei quantensprungen”. In: *Annalen der Physik* 401.3 (1931), pp. 273–294.

[14] Hermann A Haus, James G Fujimoto, and Erich P Ippen. “Analytic theory of additive pulse and Kerr lens mode locking”. In: *IEEE Journal of quantum electronics* 28.10 (1992), pp. 2086–2096.

[15] Gerhard Herzberg. “Molecular spectra and molecular structure. Vol. 1: Spectra of diatomic molecules”. In: *New York: Van Nostrand Reinhold* (1950).

[16] Leo Hollberg et al. “Atomic clocks of the future: using the ultrafast and ultrastable”. In: *International Conference on Ultrafast Phenomena*. Optica Publishing Group. 2002, MA1.

[17] Peter Horak and Francesco Poletti. “Multimode nonlinear fibre optics: Theory and applications”. In: *Recent Progress in Optical Fiber Research* 3 (2012).

[18] Zhihua Huang et al. “Combined numerical model of laser rate equation and Ginzburg-Landau equation for ytterbium-doped fiber amplifier”. In: *JOSA B* 29.6 (2012), pp. 1418–1423.

[19] Johan Hult. “A fourth-order Runge-Kutta in the interaction picture method for simulating supercontinuum generation in optical fibers”. In: *Journal of Lightwave Technology* 25.12 (2007), pp. 3770–3775.

[20] F.O. Ilday et al. “Self-similar evolution of parabolic pulses in a laser”. In: *Physical review letters* 92.21 (2004), p. 213902.

[21] WGCGB Kaiser and CGB Garrett. “Two-photon excitation in Ca F 2: Eu 2+”. In: *Physical review letters* 7.6 (1961), p. 229.

[22] SMJ Kelly. "Characteristic sideband instability of periodically amplified average soliton". In: *Electronics Letters* 8.28 (1992), pp. 806–807.

[23] Wayne H Knox. "Ultrafast technology in telecommunications". In: *IEEE Journal of Selected Topics in Quantum Electronics* 6.6 (2000), pp. 1273–1278.

[24] Vladimir I. Kruglov and John D. Harvey. "Asymptotically exact parabolic solutions of the generalized nonlinear Schrodinger equation with varying parameters". In: *J. Opt. Soc. Am. B* 23.12 (2006), pp. 2541–2550.

[25] Heng Li, Dimitre G Ouzounov, and Frank W Wise. "Starting dynamics of dissipative-soliton fiber laser". In: *Optics letters* 35.14 (2010), pp. 2403–2405.

[26] Robert Lindberg et al. "Accurate modeling of high-repetition rate ultrashort pulse amplification in optical fibers". In: *Scientific reports* 6.1 (2016), pp. 1–10.

[27] Wei Liu et al. "Pre-chirp managed nonlinear amplification in fibers delivering 100 W, 60 fs pulses". In: *Optics letters* 40.2 (2015), pp. 151–154.

[28] Francesco Poletti and Peter Horak. "Description of ultrashort pulse propagation in multimode optical fibers". In: *JOSA B* 25.10 (2008), pp. 1645–1654.

[29] WH Renninger, A Chong, and FW Wise. "Dissipative solitons in normal-dispersion fiber lasers". In: *Physical Review A* 77.2 (2008), p. 023814.

[30] WH Renninger, A Chong, and FW Wise. "Dissipative solitons in normal-dispersion fiber lasers: exact pulse solutions of the complex ginzburg-landau equation". In: *Nonlinear Photonics*. Optical Society of America. 2007, JWBPDP3.

[31] William H Renninger, Andy Chong, and Frank W Wise. "Pulse shaping and evolution in normal-dispersion mode-locked fiber lasers". In: *IEEE Journal of Selected Topics in Quantum Electronics* 18.1 (2011), pp. 389–398.

[32] Albert Schliesser, Nathalie Picque, and Theodor W Hansch. "Mid-infrared frequency combs". In: *Nature photonics* 6.7 (2012), pp. 440–449.

[33] Pavel Sidorenko, Walter Fu, and Frank Wise. "Nonlinear ultrafast fiber amplifiers beyond the gain-narrowing limit". In: *Optica* 6.10 (2019), pp. 1328–1333.

[34] Pavel Sidorenko, Walter Fu, and Frank W Wise. "Gain-managed nonlinear fiber amplifier". In: *The European Conference on Lasers and Electro-Optics*. Optical Society of America. 2019.

[35] Pavel Sidorenko and Frank Wise. "Generation of 1 μJ and 40 fs pulses from a large mode area gain-managed nonlinear amplifier". In: *Optics Letters* 45.14 (2020), pp. 4084–4087.

[36] Daniel B Soh, Johan Nilsson, and Anatoly B Grudinin. "Efficient femtosecond pulse generation using a parabolic amplifier combined with a pulse compressor. II. Finite gain-bandwidth effect". In: *JOSA B* 23.1 (2006), pp. 10–19.

[37] Xinyang Su et al. "A compact high-average-power femtosecond fiber-coupled two-color CPA system". In: *IEEE Journal of Selected Topics in Quantum Electronics* 24.5 (2018), pp. 1–5.

[38] Frank W Wise, Andy Chong, and William H Renninger. "High-energy femtosecond fiber lasers based on pulse propagation at normal dispersion". In: *Laser & Photonics Reviews* 2.1-2 (2008), pp. 58–73.

[39] Yoann Zaouter et al. "Stretcher-free high energy nonlinear amplification of femtosecond pulses in rod-type fibers". In: *Optics letters* 33.2 (2008), pp. 107–109.

Appendix A

Simulated and Experimental Comparisons

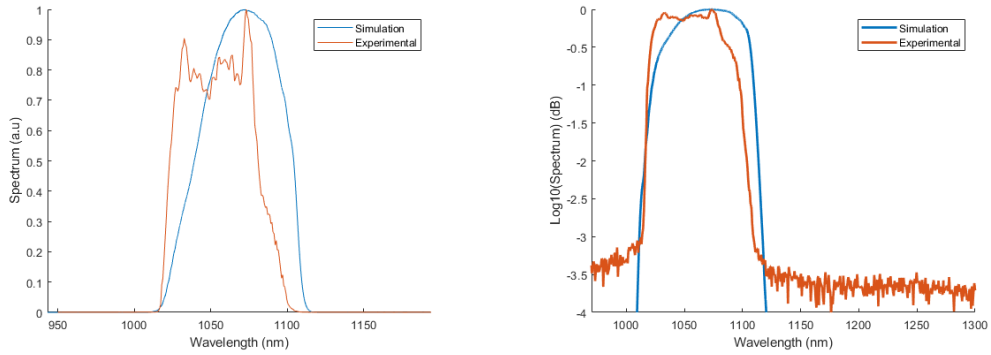

(a) 1W pump power

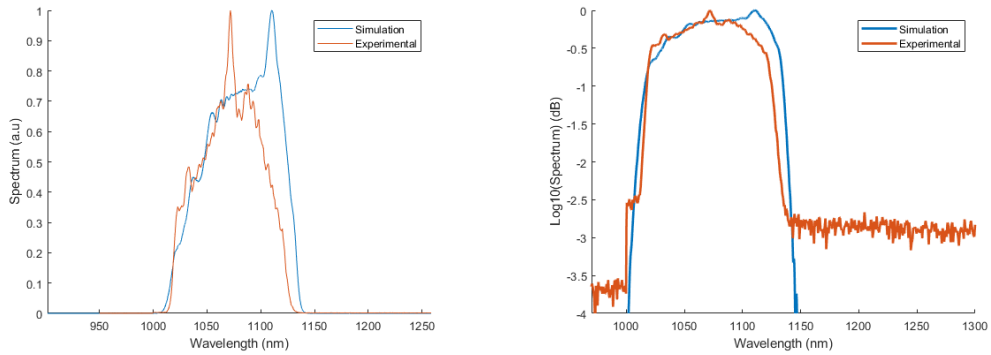

(b) 2W pump power

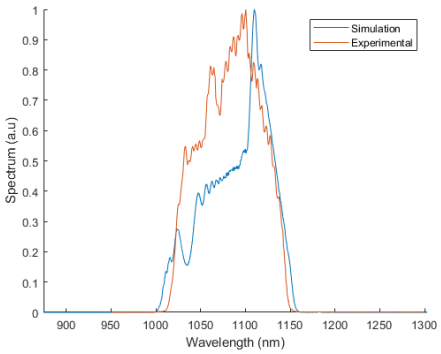

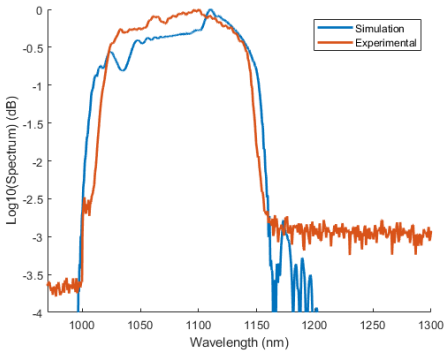

(c) 3W pump power

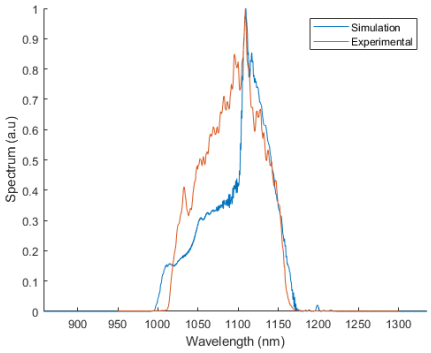

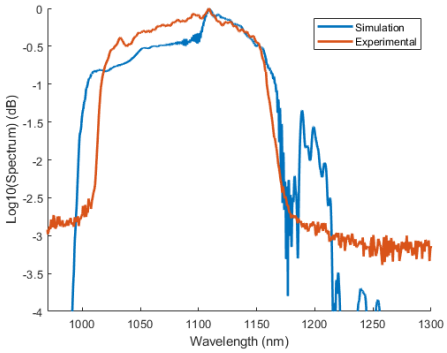

(d) 4W pump power

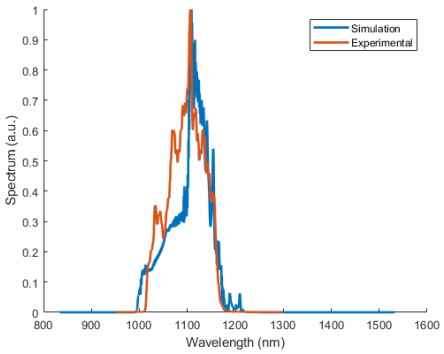

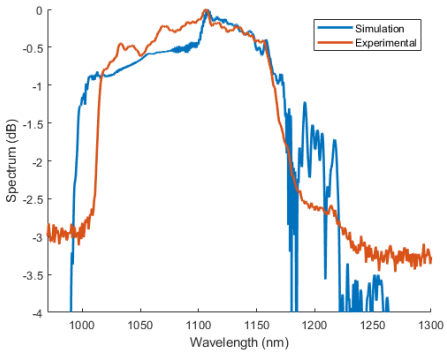

(e) 4.5W pump power

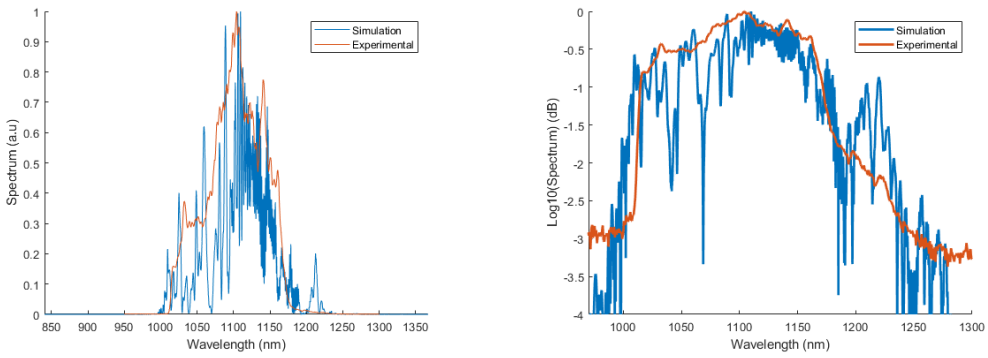

(f) 5W pump power

Figure A.1: A comparison of the simulated and experimental spectra of the GMNA at various pump levels. Linear plots are on the left and log plots on the right.